

Drew University  
College of Liberal Arts

**Nutrient Availability in the Ocean:  
An analysis of 2-nitrophenol on iron containing mineral dust and the effects of nutrients on  
phytoplankton distribution in the Southern Ocean.**

A Thesis in Chemistry

By

Hannah Primiano

Submitted in Partial Fulfillment  
Of the Requirements  
For the Degree of  
Bachelor of Science  
With Specialized Honors in Chemistry

May 2022

## Acknowledgements

I have had a wonderful support system throughout my time at Drew and I would like to thank all my friends, family, professors, and mentors for their help and support. Everything that I have accomplished is due to the support of all of the people who have believed in me. Drew has provided a wonderful learning environment, and my professors have supported me every step of the way. Dr. Mary Ann Pearsall and Dr. Ryan Hinrichs have been wonderful mentors since my freshman year. They have both believed in me, encouraged me, and trusted me to pursue chemistry even when I wasn't sure I could. Dr. Lisa Jordan has been so helpful and supportive throughout this thesis process and my time at Drew. Additionally, the support that I have received from the entire chemistry department as a whole has been instrumental to my success. Every professor that I've had and haven't had, has been kind, helpful and supportive. I would also like to thank my mentor, Dr. Barney Balch, for the encouragement to expand my horizons and for introducing me to the field of oceanography. Despite having not met me in person yet, he believed that I could travel to the Southern Ocean and do research that I had no prior knowledge of. I would like to thank the entire Balch research group: Dave Drapeau, Bruce Bowler, Sunny Pinkham, Ben Gustafson, and Giuliana Viglione as well as the other labs that participated in the RR2004 cruise for their welcoming support and friendship.

I would also not be where I am today without my family and friends. My family have always supported me in my academic endeavors no matter how crazy. Thank you to my mom and dad, for their endless love and support, and my sister, Madelyn, for her encouragement. Also, special thank you to my uncle who helped us cold weld a piece of broken lab equipment. My lab mates in the Hinrichs lab have become wonderful and valued friends. Thank you to Mason Scher,

Hunter Muratore, and Virginia Gaylord. Mason was one of the first people to introduce me to lab work in general and helped spur my interest in this topic. An additional thank you to all my friends outside of chemistry and my roommates who remind me to take a break from studying every now and then. I could not have done any of this without these people and their support. Thank you.

## Abstract

Mineral dust that enters the atmosphere becomes a major source of iron and other limiting nutrients that determine phytoplankton growth and distribution in the ocean. Reactions of mineral dust by trace organic gases found in the atmosphere can affect the amount of soluble and bioavailable iron. This process is known as atmospheric processing. Understanding the atmospheric processing of iron rich mineral dusts can help atmospheric and nutrient models become more accurate. Nutrient availability, which can be affected by mineral dusts, directly correlates with phytoplankton distribution. In this paper, we will compare the mineral dust properties and the phytoplankton distribution to increase our understanding of nutrient availability in global oceans. The first study is between the interactions of 2-nitrophenol (2NP), a known biomass burning product and pollutant, with nontronite, an iron rich clay. Diffuse Reflectance Infra-Red Fourier Transform Spectrometry (DRIFTS) identified physisorbed 2NP to be the main product. There was no observation of 2NP undergoing photolysis, despite that being an important gas phase mechanism. We also identified the presence of co-adsorbed water to minimally affect the concentration of surface adsorbed 2NP. The second study in this work is an analysis of phytoplankton distribution in the South Indian Sector of the Southern Ocean in relation to nutrient levels. Our findings show that coccolithophores significantly correlate with silicate levels in the area. This could point to silicate pathways within coccolithophores that have previously gone underrepresented. The implications of each of these topics allow us to build on existing models of mineral dust dissolution and give us a better idea of mechanisms that are affecting nutrient distribution and uptake.

## Table of Contents

<b>Chapter 1: Introduction.....</b>	<b>1</b>
<i>1.1: An overview of atmospheric and ocean interactions .....</i>	<i>1</i>
<i>1.2 Global atmospheric particle distribution .....</i>	<i>3</i>
<i>1.3: Phytoplankton and Global Ocean Nutrient Cycling.....</i>	<i>6</i>
<i>1.4: This work .....</i>	<i>10</i>
<b>Chapter 2: Atmospheric adsorbance of 2-nitrophenol on nontronite.....</b>	<b>11</b>
<i>2.1: Introduction.....</i>	<i>11</i>
<i>2.2: Methods .....</i>	<i>17</i>
<i>2.3: Results.....</i>	<i>20</i>
<b>Chapter 3: Oceanographic distribution of phytoplankton and their nutrients .....</b>	<b>31</b>
<i>3.1: Introduction.....</i>	<i>31</i>
<i>3.2: Methods .....</i>	<i>40</i>
<i>3.3: Results.....</i>	<i>47</i>
<b>Chapter 4: Discussion .....</b>	<b>52</b>
<i>4.1: A review .....</i>	<i>52</i>
<i>4.2: Relationship between the two projects.....</i>	<i>53</i>
<i>4.3: Future Research.....</i>	<i>57</i>
<b>Bibliography .....</b>	<b>58</b>

## Chapter 1: Introduction

### *1.1: An overview of atmospheric and ocean interactions*

Most Earth systems are interconnected. The atmosphere and oceans are one such interconnected system that relies on each other for global processes. Productivity is a way to measure an ecosystem by looking at the rate of generation of biomass. For example, a productive ecosystem, like a rainforest, has a lot of biomasses created in the form of plant growth etc. One of the most interesting connections between the ocean and atmosphere involves ocean productivity. The primary producers of the ocean, phytoplankton, determine most of the ocean's productivity. Phytoplankton are microscopic plants in the ocean. The productivity of phytoplankton is heavily reliant on nutrient availability. If nutrients needed for growth are not available, productivity is decreased. Limiting nutrients are compounds that are usually in small amounts that control population growth of a species.

Nutrients can be made available in the ocean from fluvial runoff, upwelling from the ocean floor, or by mineral dust, atmospheric interactions, and aerosols. Fluvial runoff refers to the transport of nutrients from rivers that get dumped into the ocean. Upwelling of water from the ocean floor can carry minerals and nutrients from the ocean floor sediment. Atmospheric mineral dusts get picked up by wind into dust storms that get carried out over the ocean. Mineral dust can stay up in the atmosphere for weeks until it eventually settles out. Mineral dust transport is extensive with dust from the Sahara Desert making it all the way to North America. When the dust settles out over the ocean, nutrients, and compounds that phytoplankton rely on can dissolve in the water to be taken up by biota later. Thus, global transport of mineral dust is an extremely important process for the deposition of nutrients and compounds into parts of the ocean that may be lacking

in these compounds. Iron is one of the major limiting nutrients in the ocean and has been shown to control phytoplankton growth and productivity.<sup>1</sup> Global transport of mineral dust involves multiple chemical interactions that can affect mineral deposition and thus the biological activity in the ocean at the primary level.

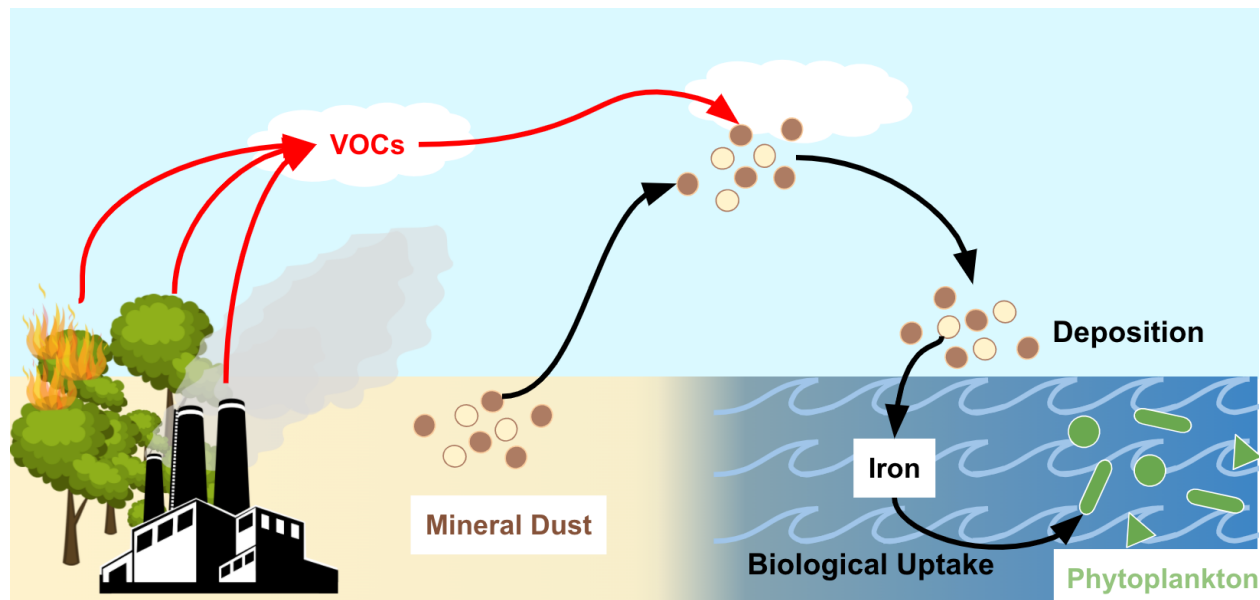


Figure 1.1: The figure above shows the general movement of mineral dust and its interactions in the atmosphere and the ocean. Three sources of VOCs, biomass burning, pollution and plants, are shown on the left.

This work will be summarizing both atmospheric and oceanic implications of mineral dust as a source of limiting nutrients. We will look at the interactions of the mineral dust and its atmospheric lifetimes and interactions. Additionally, we will look at the ocean productivity and how it is affected by nutrient availability. Figure 1.1 shows how these two aspects relate to each other. The mineral dust interacts in the atmosphere with volatile organic compounds (VOCs) and

eventually deposit iron in the ocean for uptake by phytoplankton. In the following chapters, I will describe two experiments. The first laboratory experiment focuses on mineral dust atmospheric interactions, while the second focuses on the field work analysis of phytoplankton distribution related to nutrient availability. We will begin with a brief overview of some of the factors that affect this mineral transport process.

### ***1.2 Global atmospheric particle distribution***

This process shown in Figure 1.1 begins with the emission of mineral dust into the atmosphere. Atmospheric mineral dusts are a broad category. Mineral dusts generally come from weathering and erosion of desert areas. Production of mineral dust aerosol is dependent on vegetation, precipitation and humidity, rock surface and properties, along with several other factors. Atmospheric dusts have an average diameter of  $2\mu\text{m}$ , which allows them to remain in the atmosphere for up to a few weeks.<sup>2</sup> However, the range of the particle size can vary tremendously, with larger particles settling out faster than smaller particles. Depending on mineral type and soil or rock source, mineral dust size varies. Most models divide these minerals into clay, silt, and sand. Clays are the smallest categories ranging from  $0.01\mu\text{m}$  to a maximum of  $2\mu\text{m}$ . Silts range generally from  $2\text{-}25$  or  $50\mu\text{m}$  but can change or be divided into subcategories depending on the study. Lastly, sands are anything greater than  $50\mu\text{m}$ , generally up to  $2000\mu\text{m}$ .<sup>3</sup> Sands and larger silts do not last long in the atmosphere and are not studied as much as clays and smaller silts that will likely stay in the atmosphere for weeks. Particle size of specific minerals are collected and shown in Table 1.

Mineral examples	Composition	Density (g/mL)	Average Particle Diameter ( $\mu\text{m}$ )	Clay (C) or Silt (S)
Illite	$(\text{K}, \text{H}_3\text{O}) (\text{Al}, \text{Mg}, \text{Fe})_2 (\text{Si}, \text{Al})_4 \text{O}_{10} [(\text{OH})_2, (\text{H}_2\text{O})]$	2.75	5-10	C
Kaolinite	$\text{Al}_2(\text{OH})_4\text{Si}_2\text{O}_5$	2.63	10	C
Smectite				
Nontronite	$\text{Na}_{0.3}\text{Fe}^{+3}_2(\text{Si}, \text{Al})_4\text{O}_{10}(\text{OH})_2 n\text{H}_2\text{O}$	2.57	5-10	C
Montmorillonite	$(\text{Na}, \text{Ca})_{0.33}(\text{Al}, \text{Mg})_2(\text{Si}_4\text{O}_{10})(\text{OH})_2 n\text{H}_2\text{O}$			
Calcite	$\text{CaCO}_3$	2.71	3	C & S
Quartz	$\text{SiO}_2$	2.67	>50	C & S
Feldspar				
Potassium	$\text{K}(\text{AlSi}_3)\text{O}_8$	2.68	5-10	S
Plagioclase	$(\text{Na}, \text{Ca})(\text{Al}, \text{Si})_4\text{O}_8$		10	
Gypsum	$\text{CaSO}_4 2\text{H}_2\text{O}$	2.31	3-5	S
Iron Oxides				
Hematite	$\text{Fe}_2\text{O}_3$	4.77	0.5-1	C & S
Goethite	$\text{Fe}^{+3}\text{O}(\text{OH})$			

Table 1: Common dust mineral properties are described. Minerals were chosen using the same convention as Claquin et al<sup>4</sup> and Perlwitz et al.<sup>5</sup> Most particle diameter was approximated from data obtained in Moroccan mineral aerosol dust.<sup>6</sup> Clay particles diameter was also determined from a study by Veghte et al.<sup>7</sup>

Variation in mineral dust composition determines nutrient availability. When deposited in the ocean, nutrients such as iron can be deposited, but it is dependent on the mineral structure. Most deserts contain dusts primarily comprised of silicates. However, many metals like iron, aluminum, zinc, etc. are present in mineral dusts. They can be present as counter ions or within the structure of the mineral. Iron is one of the more important metals to observe in mineral dust because it is a limiting nutrient for primary producers in the ocean.<sup>1</sup> Only approximately 3.5% of global dust contains iron<sup>2</sup>, not all of which makes it to the ocean. Common iron containing minerals include iron oxides (goethite, hematite, magnetite) and iron containing clays (nontronite, montmorillonite). Nontronite and montmorillonite are a part of a larger category of clays called smectites. Solubility is one of the most important factors for iron availability in the ocean. While in soil, approximately 0.5% of the iron is soluble, but after being in the atmosphere, it can be up to 80% soluble.<sup>8</sup> Factors that increase solubility can include, organic complexation in the atmosphere, photochemistry, pH, and other factors.<sup>2</sup> Complexation and photochemistry can lead to a change in oxidation state for iron from Fe(III) to Fe(II), which increases solubility and availability to biota. This has been shown with oxalic acid and other acids.<sup>8</sup> This will be discussed more in chapter 2.

### 1.3: Phytoplankton and Global Ocean Nutrient Cycling

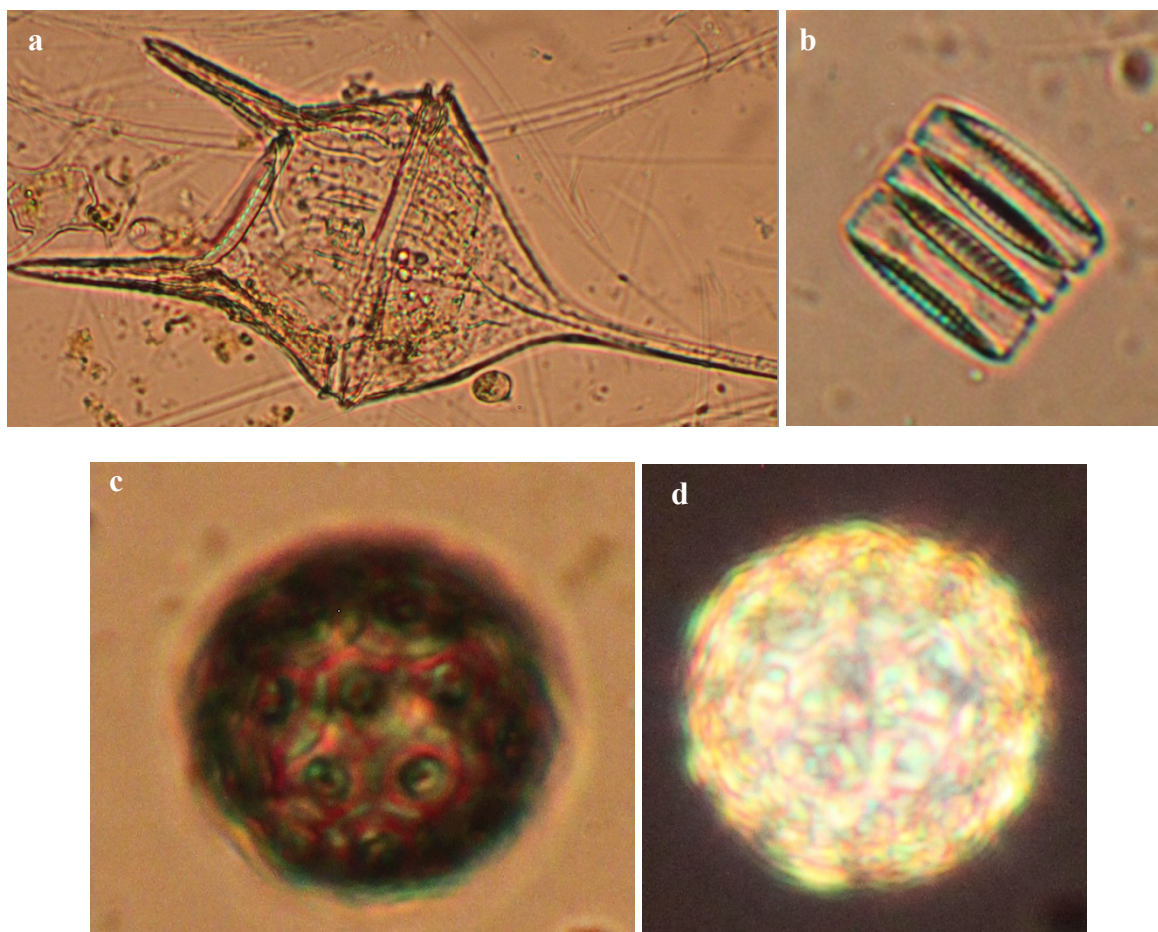


Figure 1.2: This figure shows three major types of phytoplankton that will be discussed throughout the work as well as key identifying features. Images were taken by Dr. William Balch.

In addition to iron, different mineral dusts can settle out in the ocean and deposit important nutrients such as phosphorus or ions like calcium, potassium, magnesium, etc. Variations in phytoplankton species allow for variation in nutrient uptake due to the different needs of each species. We focus on three groups of phytoplankton: coccolithophores, diatoms, and dinoflagellates shown in Figure 1.2. These three types are major classifications of phytoplankton that can be easily distinguished from each other based on shape and properties. Image (a) is a

ceratium dinoflagellate, which is a specific type of dinoflagellate. Most, if not all, dinoflagellates are identifiable by a girdle, which is the ridge along the middle of the phytoplankton. Image (b) is a group of three diatoms stacked on each other. Diatoms are identified by their symmetry. They can also often be found linked together, like what is shown in the image. Image (c) and (d) are the same image of a coccolithophore. Image (c) is under visible light, and (d) is under polarized light. Coccolithophores reflect polarized light which allows the primary identification method for coccolithophores to be relatively easy. Each of these three phytoplankton have many species that fall under the category, but for the purposes of this paper, we will be looking at the categories based on genus.

Coccolithophores and diatoms both make external structures, but they use different minerals. In this case, coccolithophores use calcium carbonate and diatoms use silica as shown in Figure 1.3. Coccolithophores have individual plates, called coccoliths, that are formed through biomineralization. They are visible as overlapping circles that surround the coccolithophore, such as that in Figure 1.2c. Diatom frustules are not separate plates but instead are more similar to a shell. Species variation in frustule and coccolith shape are common.

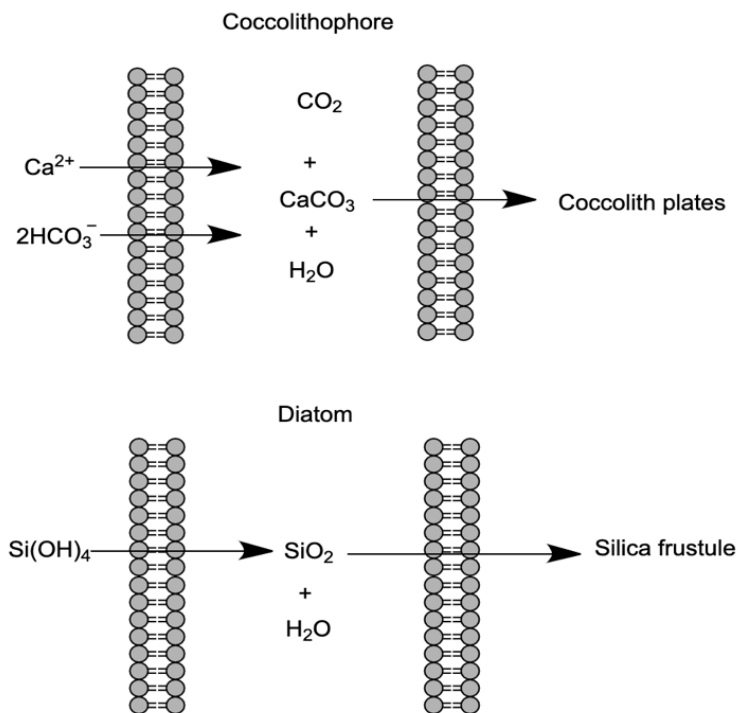


Figure 1.3: The schematic shows the general intake of minerals and ions to create external structures for coccolithophores (top) and diatoms (bottom).

Similarly, species variations also contribute to how much of a certain type of nutrient different phytoplankton will need. An important nutrient across all species however is iron because iron has been identified as a major limiting nutrient in the ocean and an important nutrient for phytoplankton productivity. Ocean productivity is an important measure of the health of our oceans and single-celled phytoplankton are the main contributors to the ocean's productivity.<sup>9</sup> As the primary producers of the ocean, they are the base of the oceanic food web. However, their importance is greater than their own immediate ecosystem. Due to their distribution and population size, phytoplankton contribute approximately 20% of the Earth's oxygen.<sup>10</sup> Phytoplankton also

participate in multiple global processes, such as global ocean nutrient regulation and carbon sequestration.

Nutrient availability is one of the most important factors to determine phytoplankton distribution. This work focuses on iron, silicates, nitrates, nitrites, phosphates, and ammonium. Nutrient sources in the ocean vary based on geographic location. Geographic location impacts nutrient availability, light availability, temperature, salinity, etc. Phytoplankton need specific conditions in terms of these variables to live. In general, areas of low nutrients and/or low light availability are not conducive to phytoplankton survival. To understand general distribution of all phytoplankton, we can examine nutrient availability. For example, the open ocean is lower in nutrients while the coastal regions have higher concentrations due to runoff allowing for greater populations near coastal regions. By relating nutrient availability and phytoplankton distribution, we can better understand and predict global distribution and productivity.

To understand productivity and plankton distribution, we must also remember that water masses are constantly moving and cycling over large time scales. Bottom or deep water can gather nutrients from ocean sediments, hydrothermal vents, and detritus. This nutrient rich water can eventually provide an area for phytoplankton to grow when it surfaces. Thus, phytoplankton are more likely to be in areas where upwelling occurs. The equator and Southern Ocean (SO) are great examples where nutrient availability due to upwelling, allows for increased plankton growth.

#### ***1.4: This work***

Nutrient availability in the ocean is a key determinant of ocean productivity by controlling the populations of phytoplankton. The goal of this work is to connect two different projects into the larger context of ocean-atmosphere interactions. We combine the efforts of two laboratories as well as laboratory models and field work data into this cohesive paper to connect the two concepts.

The first project, detailed in chapter 2, seeks to determine the chemistry that happens between organic gases and mineral dusts. It also seeks to determine the chemical mechanisms that govern these interactions and the iron dissolution from iron-containing mineral dusts. 2-nitrophenol (2NP) is a photoreactive organic molecule that is often a product of biomass burning and pollution. For this reason, we look at the interactions that occur between 2NP and nontronite, an iron containing clay, as a general model for possible atmospheric interactions. These types of interactions occur in the atmosphere every day, which can influence the state of iron and the surface area of the mineral dust, further influencing iron dissolution.

The second project, discussed in the third chapter, focuses on the distribution phytoplankton in the Southern Ocean (SO), which is a primarily iron deficient region of the ocean. By, collecting data on the abundance of three major categories of phytoplankton and the nutrients in the area, we can better understand the significance of limiting nutrients in the SO. Together this research can help us understand the interconnectedness of the atmosphere-ocean interactions and hopefully allow us to determine how this research should continue to be studies.

## Chapter 2: Atmospheric adsorbance of 2-nitrophenol on nontronite

### 2.1: Introduction

The interactions of mineral dust and atmospheric trace gases are integral in the formation of secondary organic aerosols, secondary volatile organics, and biologically relevant nutrients. Relevant atmospheric gases include volatile organic compounds, ozone, NO<sub>2</sub>, sea spray aerosols, etc. These molecules can come from multiple sources, including pollution, biomass burning, plant emissions, and other atmospheric reactions. Literature studies of mineral dust interactions are numerous and include studies on the interactions of atmospherically relevant molecules, such as catechol<sup>11,12,13</sup>, nitrophenols<sup>14,15,16</sup>, nitrocresols<sup>14</sup>, oxalate<sup>17,18</sup>, sulfuric acid<sup>18</sup>, acetic acid<sup>18</sup>, HNO<sub>3</sub><sup>19</sup>, and NO<sub>2</sub><sup>19</sup> on different mineral dusts. Atmospheric processing of mineral dusts by these molecules has the potential to change properties of the mineral dust such as surface area<sup>18</sup> and oxidation state. In turn, the changes to mineral dust properties affect solubility when deposited in the ocean.

### *Mineral Dust*

Mineral dust is an umbrella term for a classification of dusts that vary based on composition, size, and properties. When analyzing the global mineral dust distribution, we can see that the majority of deserts and other sources of atmospheric mineral dust are high in silica and titanium oxide containing minerals.<sup>20</sup> However, the most biologically relevant dusts are high in iron. Aeolian mineral dust is a large source of oceanic iron, which is an important limiting nutrient for phytoplankton. Atmospherically relevant mineral dust depends on particle size, because larger particles will settle out of the atmosphere faster. For this reason, iron rich clays, like smectites, are

a good area of focus. Clays are generally smaller, with smectites having an average particle size of  $3 \mu\text{m}^7$  and can therefore have a longer atmospheric lifetime than larger particles. For this paper, we will be focusing on nontronite, which is shown in Figure 2.1.

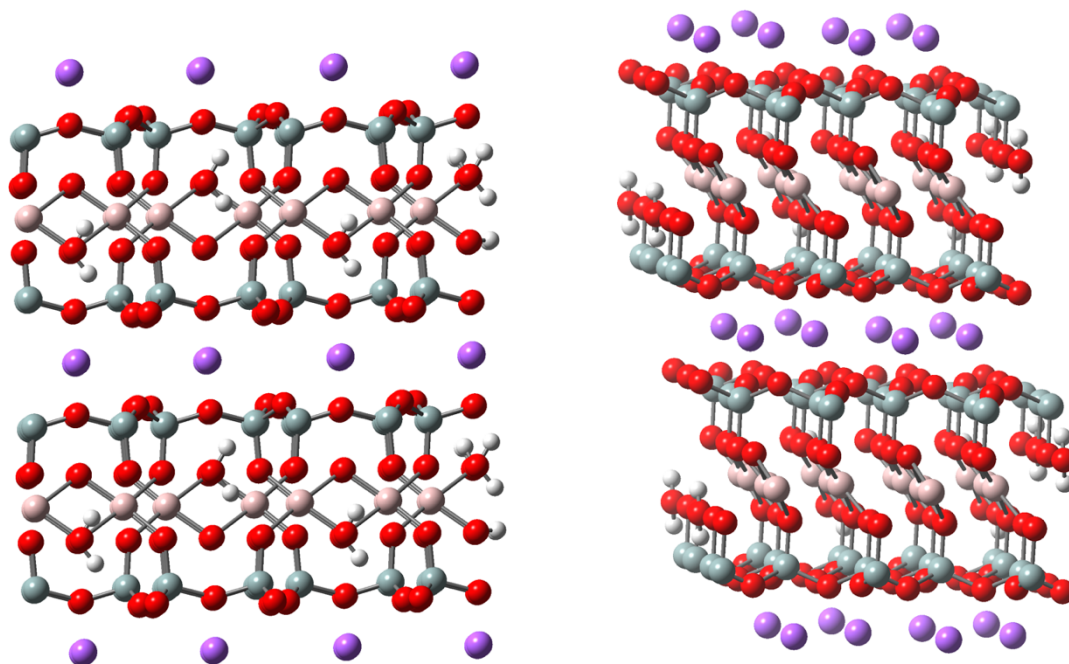


Figure 2.1: A schematic of the nontronite structure is provided to the left. Image a is the front view of the structure. Image b is the side view of the system. The side view provides a good view of the OH groups that can be bound to the iron on the edge. The pink atoms are irons, the red atoms are oxygens, the grey atoms are silica, the white atoms are hydrogens, and the purple circles are counter ions. The specific nontronite that we obtained may also have some iron in tetrahedral configurations, but the primary configuration is octahedral irons.<sup>21</sup>

## *Nitrophenol*

As a prominent photoreactive biomass burning product, 2-Nitrophenol (2NP) is likely to be an interesting example of chemistry on the surface of mineral dust. Nitrophenols can come from many sources including emissions from several industries and as a product of other atmospheric reactions. Previous studies, such as Wang et al., have shown that the nitrophenol diurnal cycles align with biomass burning.<sup>14</sup>

Nitrophenols are known photoreactive chemicals that absorb light around 370nm. 2NP has an absorption maximum at 332nm in the gas phase and 345-367nm when adsorbed to a dust surface.<sup>15</sup> Aqueous and gas phase photochemical reactions show that nitrophenols including 2NP can come from products such as HONO, or nitric acid.<sup>22</sup> HONO is a pollutant and can form the hydroxyl radical, which is an important reactant in the formation of ozone. In an aqueous solution, different nitrophenols produce different quantum yields depending on pH and wavelength, with 2NP producing more HONO at more basic pHs.<sup>23</sup> In the gas phase, it has also been shown that 2NP can form HONO. Bejan et al.<sup>22</sup> proposed a similar mechanism to the one depicted in Figure 2.2, which is consistent with literature observations of 2NP when exposed to light or heat. If this reaction is possible, it is reasonable for us to ask what reactions may be possible if 2NP is adsorbed onto the surface of a mineral dust such as nontronite. Do the photochemical properties of 2NP change or impact the nontronite structure in any way?

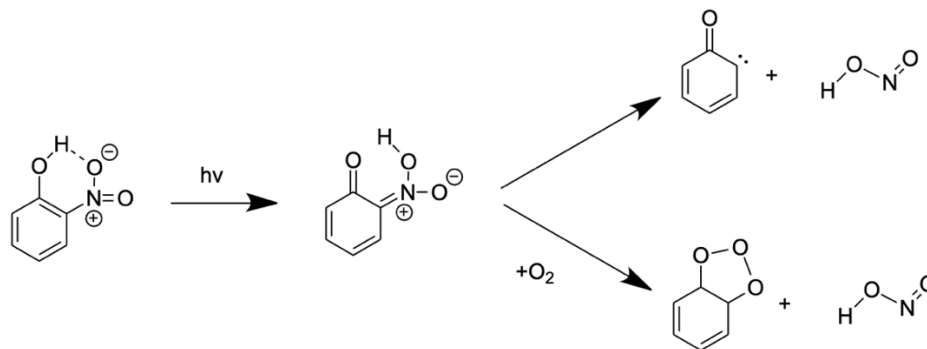


Figure 2.2: The reaction scheme shows the proposed formation of HONO from 2NP when exposed to light.

Even without photochemistry occurring, there are other possible types of interactions that can still happen with organics on aerosols. Two methods of interaction that can result from the coating of a solid with a chemical are physisorption and chemisorption. Figure 2.3 depicts the possible outcomes of 2NP adsorbing onto an iron containing dust in both a physisorption and chemisorption scenario. Physisorption occurs when hydrogen bonding or other intermolecular forces cause some interactions and adsorption to the surface. Chemisorption however has direct covalent bonding where a water molecule is lost for the molecule to adsorb. Depending on the molecule, there can be monodentate or bidentate bonding. In Figure 2.3, monodentate bonding is shown. Bidentate bonding would occur if two covalent bonds were created between the surface and the 2NP molecule. These interactions can affect the possible formation of subsequent species. For example, if chemisorption occurs, HONO will likely not be formed through the mechanism in Figure 2.1, because the oxygen on the 2NP will be covalently bonded to the iron. Additionally, other atmospherically relevant species, such as water, can impact the interactions between 2NP and nontronite.

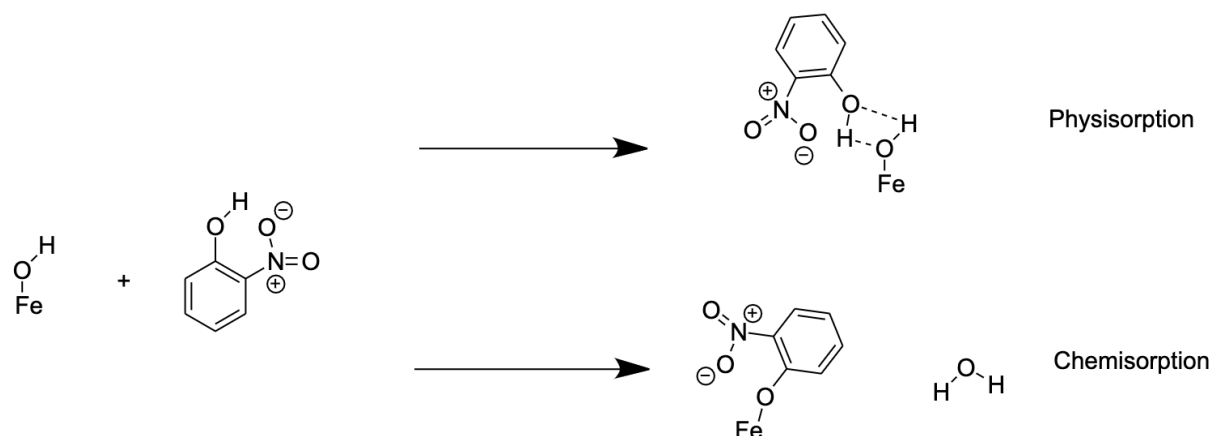


Figure 2.3: This reaction scheme shows the possible outcomes of physisorption and chemisorption on an iron containing mineral dust.

### *Atmospheric Conditions*

Mineral dust interactions with other atmospheric molecules do not occur in a vacuum. Atmospheric composition and conditions play important roles on the chemistry that takes place on the surface of mineral dusts. Of these different conditions, this work will be focusing on relative humidity (RH) and solar radiation.

RH, or the percentage of water vapor in the atmosphere, is highly variable in the atmosphere. Mineral dust enters the atmosphere over the desert in dust storms where RH is very low, but can travel far out over the ocean, where RH is very high. The increase of water molecules in the air with the increase of RH can affect which type of surface interactions occur. Generally, as water vapor increases, the number of volatile organics or other atmospheric molecules that adsorb to the surface of dust will decrease, because water molecules are adsorbing in its place. This can inhibit or alter bonding that may happen between dusts and molecules. With the addition

of water molecules, other chemicals can become solvated on the surface of the mineral dust. Overall, the addition of water can change the types and/or rates of reactions.

Light is another variable source of reactions in the atmosphere. Photochemistry in the atmosphere is a major source of radicals, which go on to encourage more reactions. Important radical reactions in the atmosphere include the hydroxyl radical which creates ozone and other important secondary organic aerosols.

### ***Nontronite and Nitrophenol Experiment***

This chapter focuses on determining the chemical interactions that are taking place in the atmospheric interactions between nontronite and 2NP. In addition to determining the processes, we seek to look at atmospherically relevant conditions by varying the relative humidity that the experiments are performed at. The last variable tested was the presence or absence of light in order to determine the photoreactive properties of nontronite in this setting. Using electronic structure and frequency calculations, we modeled the bending vibrations of 2NP to determine the type of adsorption that is occurring. Experiments were carried out using Diffuse Reflectance InfraRed Fourier Transform Spectroscopy (DRIFTS) in order to measure the 2NP and water adsorption to nontronite over time.

## 2.2: Methods

Samples of nontronite were obtained from The Source Clays Repository. Nontronite samples (Nau-2) are aluminum poor obtained from Uley Mine in South Australia.<sup>24</sup> The structural formula of the source clay is  $M^{+}_{0.72} [Si_{7.55}Al_{0.45}][Fe_{3.83}Mg_{0.05}]O_{20}(OH)_4$ .<sup>21</sup> Approximately 0.11g ( $\pm 0.03$ ) of dust was packed into a reaction chamber inserted into a Thermo Nicolet 6700 Diffuse Reflectance Infrared Fourier Transform Spectrometer (DRIFTS). The DRIFTS is equipped with a liquid nitrogen cooled MCT detector.

As shown in Figure 2.4, the setup for the experiment includes three gas flows: a dry flow, wet flow, and organic flow. The dry and wet flow both come from a single air tank. The flow rates are controlled with a MKS type 247 four channel readouts. The wet air flow line goes through a bubbler slightly filled with DI water. The organic flow comes from a nitrogen tank to avoid any oxidation that may occur with the organics and air. In this case the organic, 2NP, is introduced via a bubbler. All gases combine and are mixed in the tubing before flowing over the sample. The flow rate for the organic flow is controlled via a Matheson flow meter. Additionally, a Newport 67005 solar simulator with a xenon lamp, indicated by the sun in Figure 2.4, was positioned over the sample so that it may be turned on or off for different experiments. A mirrored tube allowed for controlled exposure of light directly onto the sample.

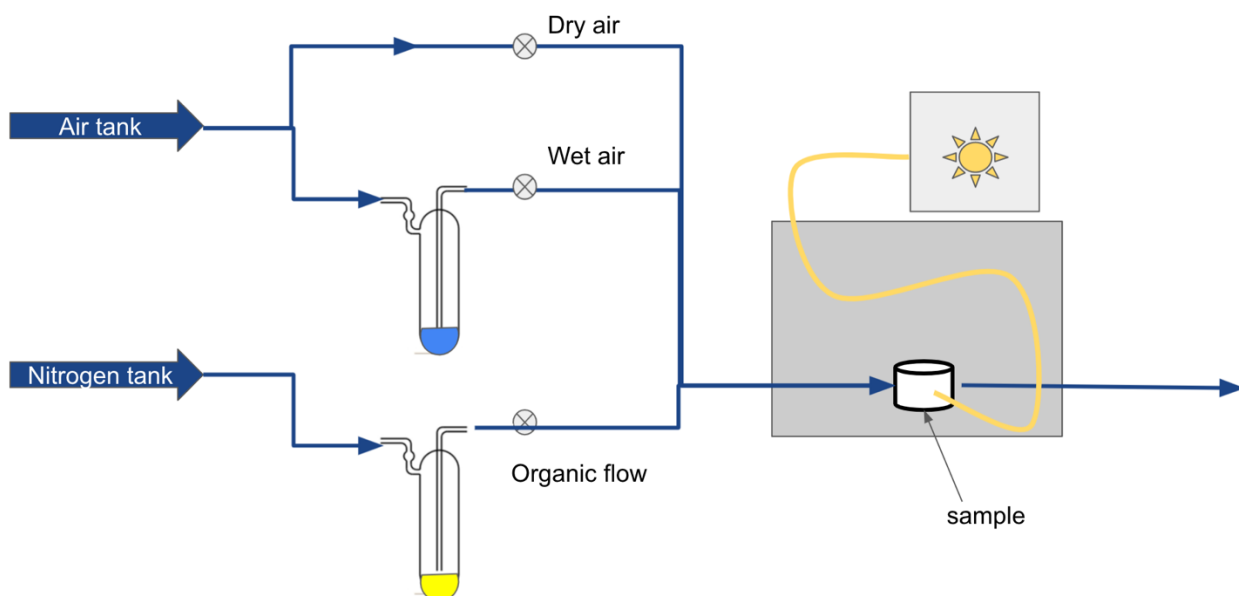


Figure 2.4: The figure shows the setup for the gas flows over the samples.

The DRIFTS was calibrated so that it collected absorbances from  $400\text{-}4000\text{cm}^{-1}$ . The nontronite sample was packed into the chamber and the dry airflow was left on overnight to ensure that the dust was completely dry. The background was taken for each sample while it was dry.

All experiments on the relative humidity of the sample were performed in the dark and the sample covered in aluminum foil. All backgrounds were taken after the clay had been left to dry out overnight with dry air flowing. Then, the chamber was isolated, and the humidity was allowed to reach a steady state in the tubing. The water bubbler was connected only for the relative humidity experiments. The chamber was then reopened, and the series was started. After about 15 minutes, the water should have reached a steady state within the chamber. At this point the chamber was isolated again and the 2NP flow was opened so that it could also reach a steady state. After 1 hour, the chamber was opened again. After 2 more hours the chamber was isolated and the 2NP flow was stopped. The air was left to get the 2NP out of the tubing. The next morning, the series was

stopped, a new series was started, and the chamber was reopened to observe desorption. Again, this was left overnight, and the next morning, the series was stopped, and the dust was collected.

When conducting light experiments, the fiberoptic tube from the xenon lamp was set and clamped in place to direct light directly into the chamber. Everything was then covered in tin foil to ensure that there is only light when it is on. To conduct the light experiments, we started collecting a series and started the flow of 2NP. After 1 hour the light was turned on and left for at least 3 hours. After turning the light off, the series was stopped, and the dust collected.

IR spectroscopy measures the molecular vibrations associated with different energies. Each peak in an IR spectrum relates to a different molecular vibration, which can include bending or stretching of bonds. If physisorption is occurring, the molecular vibrations will be different than the chemisorption. Specifically, the O-H on the 2NP will have a different stretching vibration because it will not be a part of the chemisorption product. Thus, electronic frequency calculations were performed using GaussView to determine the IR spectra for theoretical physisorption and chemisorption adsorption. The models for physisorption and chemisorption were approximated by assuming a gaseous 2NP structure and a monodentate covalent bonding of 2NP onto an iron oxide as shown in Figure 2.7. Frequency and optimization calculations were performed with the basis set DFT B3LYP 631G +d.

### 2.3: Results

#### *Adsorption of 2NP under dry conditions*

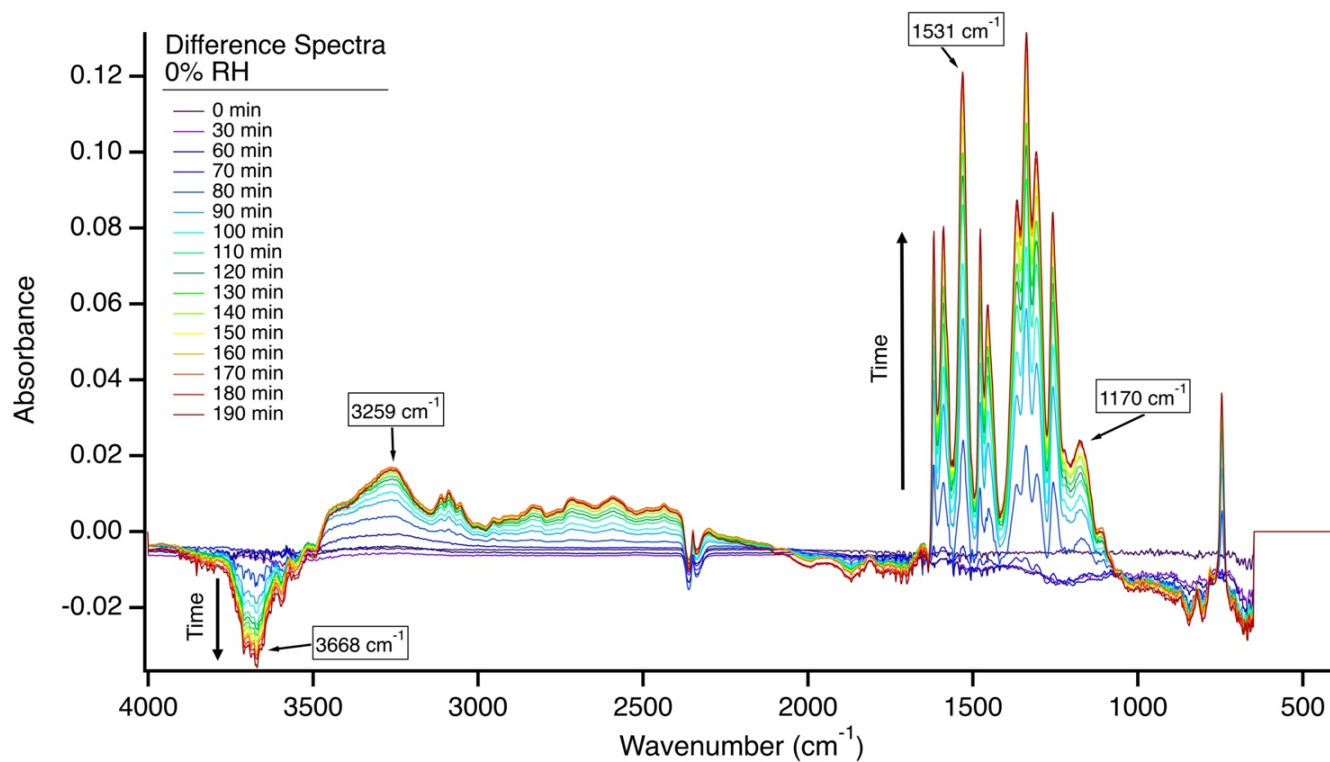


Figure 2.5: The above graph shows the difference spectra for 2NP adsorbing onto the surface of nontronite over two hours at 0% RH. Each spectrum is the absorbance subtracted from the initial spectrum to show the growth or depletion of peaks.

Label	Wavenumber ( $\text{cm}^{-1}$ )	Intensity	Description
A	3669.9	-0.0360	Surface hydroxyl free O-H stretch from Nontronite
B	3264.9	0.0164	H-bonded O-H vibration from 2NP and surface O-H
C	1618	0.0792	Asymmetric stretching within the ring of 2NP
D	1589	0.0805	Asymmetric stretching of the $\text{NO}_2$ on 2NP
E	1531	0.121	Ring hydrogens bend
F	1477	0.0799	OH bond stretch or ring hydrogen rocking
G	1454	0.0598	Asymmetric ring, O-H, and $\text{NO}_2$ stretch
H	1367	0.0874	Asymmetric ring, O-H, and $\text{NO}_2$ stretch
I	1338	0.132	Asymmetric NO bond stretch and OH bend
J	1307	0.100	Asymmetric ring, O-H, and $\text{NO}_2$ stretch
K	1257	0.0843	Ring hydrogen bend
L	1170	0.0242	Asymmetric ring stretch

Table 2.1: The above table shows the prominent peaks from left to right in Figure 2.5 and 2.8.

These peaks are recurring throughout the experiments. The labels correspond with figure 2.8.

Preliminary IR analysis was conducted on 2NP adsorbing to the surface of nontronite as shown in Figure 2.5. The main peaks are labeled from left to right in Table 2.1. This spectrum, conducted at 0% RH, highlight some changes in the O-H stretching region between 3700 and 3000  $\text{cm}^{-1}$ . Usually, O-H bond stretching occurs in the region above 3000 $\text{cm}^{-1}$  and bending appears around 1634  $\text{cm}^{-1}$  for surface adsorbed water. In this spectrum, there is no peak around 1634 $\text{cm}^{-1}$

indicating that none of the O-H bending is coming from changes in water or water vapor, which aligns with the relative humidity of 0%. Thus, any peaks that we see above  $3000\text{cm}^{-1}$  must be coming from a different O-H bond than water. The decrease in O-H stretching is likely due to a decrease in the free O-H stretching of the nontronite as 2NP began to interact with it. The interaction of the 2NP changes the stretching vibration of the O-H on the nontronite. This new vibrational frequency appears in the band from  $3500$  and  $3000\text{ cm}^{-1}$ . This is why we see the peak between  $3500$  and  $3000\text{ cm}^{-1}$  growing in as the peak around  $3600$  decreases. This region also has the addition of the O-H stretching from the 2NP, which is why it is not an inversely identical peak to the peak at  $3600\text{ cm}^{-1}$ .

The peaks in the fingerprint region, to the right of  $1600\text{ cm}^{-1}$ , are very similar to the IR spectrum for 2NP by itself.<sup>25</sup> The Figure 2.5 shows us that there is a disruption of the O-H vibrations on the surface of nontronite, presumably from interaction and adsorption of the 2NP. Both physisorption and chemisorption could have this effect of disrupting the nontronite surface O-H vibrations. Previous data has shown that there is a deprotonation happening because of the surface adsorbed 2NP.<sup>15</sup> In order to determine how 2NP is creating this deprotonation, either through physisorption or chemisorption, we conducted a multipeak fitting. A deeper analysis of the vibrations in the fingerprint region was done in the next section.

### *Gaussian calculations and Multipeak Fitting*

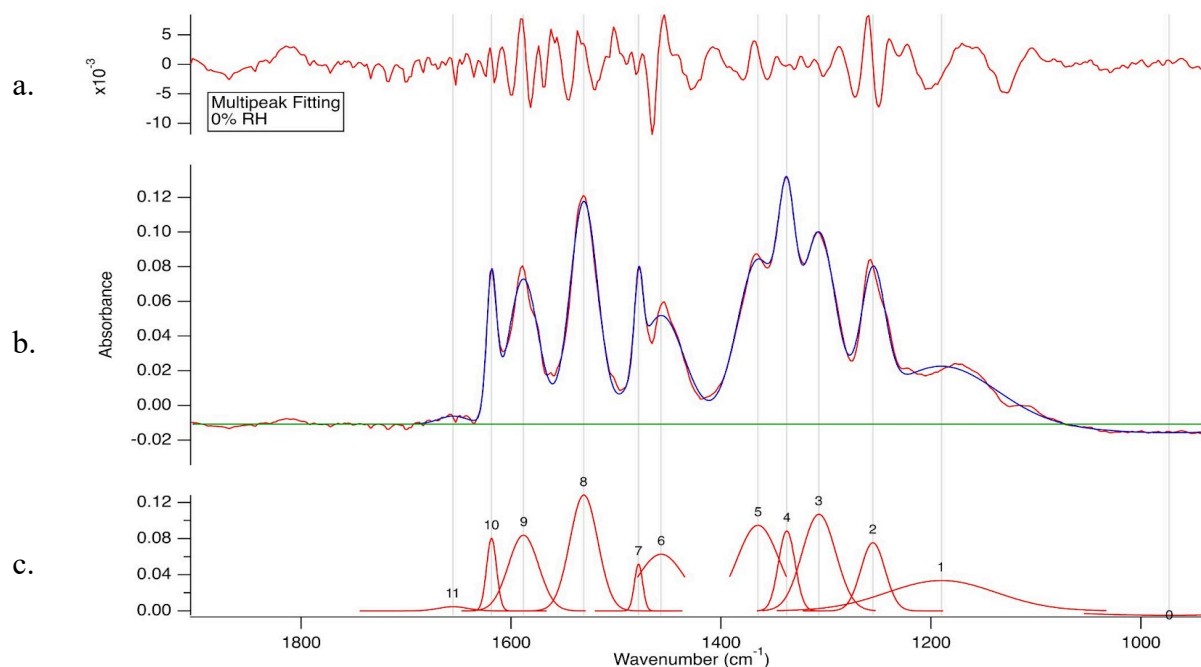


Figure 2.6: The above figure is an IGOR multipeak fitting calculation to determine the peaks that make up the final 0%RH spectrum obtained. Graph a shows the residual or difference between the fit and the original spectrum. Graph b is showing the original spectrum in red, and the calculated fit in blue. The calculated fit is coming from graph c. Graph c is show the numbered individual peaks that are making up the predicted spectrum.

A multipeak fitting calculation was performed in IGOR on the final spectrum from the 0% RH trial. Each individual vibration I made contributes a gaussian shaped peak to the spectrum. Twelve peaks were identified in the spectrum, although the first one had a negative intensity, and so this peak can be negated during further analysis. The calculated gaussian peaks are shown in Figure 2.6c. From this calculation, the vibrational frequency, absorbance intensity and area were obtained.

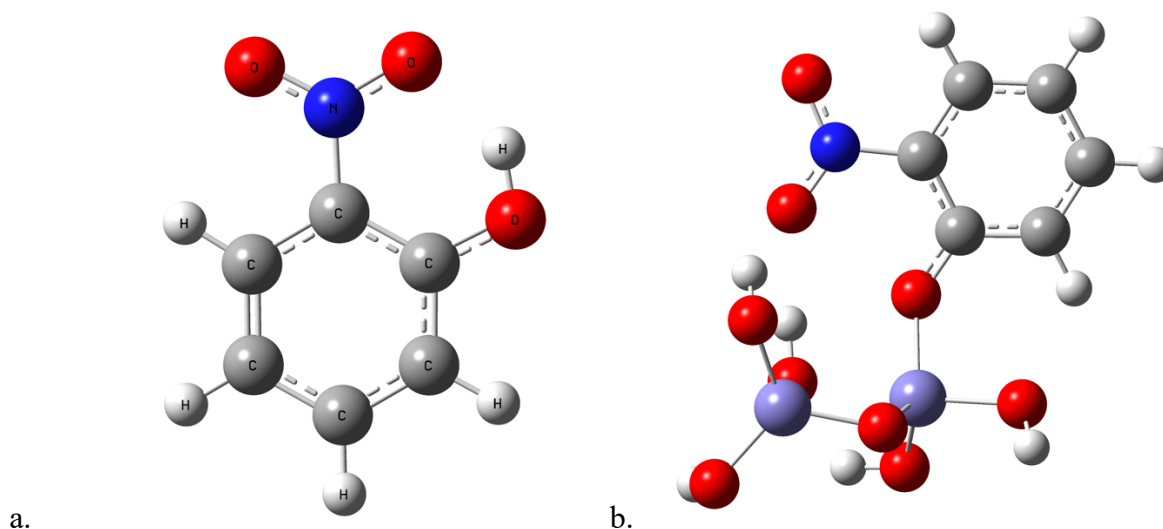


Figure 2.7: Molecule a shows the solvated gas phase 2NP the theoretical spectrum was calculated for. Molecule b shows the 2NP bonded to an iron structure that was calculated as a proxy for 2NP chemisorbed onto nontronite.

To identify the vibrational modes associated with each individual peak in the spectrum, electron structure and frequency calculations were performed using Gaussian 09 to predict the spectrum for the molecules in Figure 2.7. A theoretical spectrum of 2NP in the gas phase is the simplest model for identifying the peaks and to evaluate if there are some changes when the gas interacts with the nontronite. As a proxy for physisorption, we calculated the spectrum for molecule a in Figure 2.7. Molecule b is a theoretical proxy for the expected interaction with nontronite if chemisorption occurs.

The peaks calculated from these two molecules were compared to the original final 0% RH spectrum in Figure 2.8. The theoretical calculations performed in Gaussian only account for harmonic motion, so to account for anharmonic motion, the frequencies were scaled by 0.985 and 0.98 respectively.

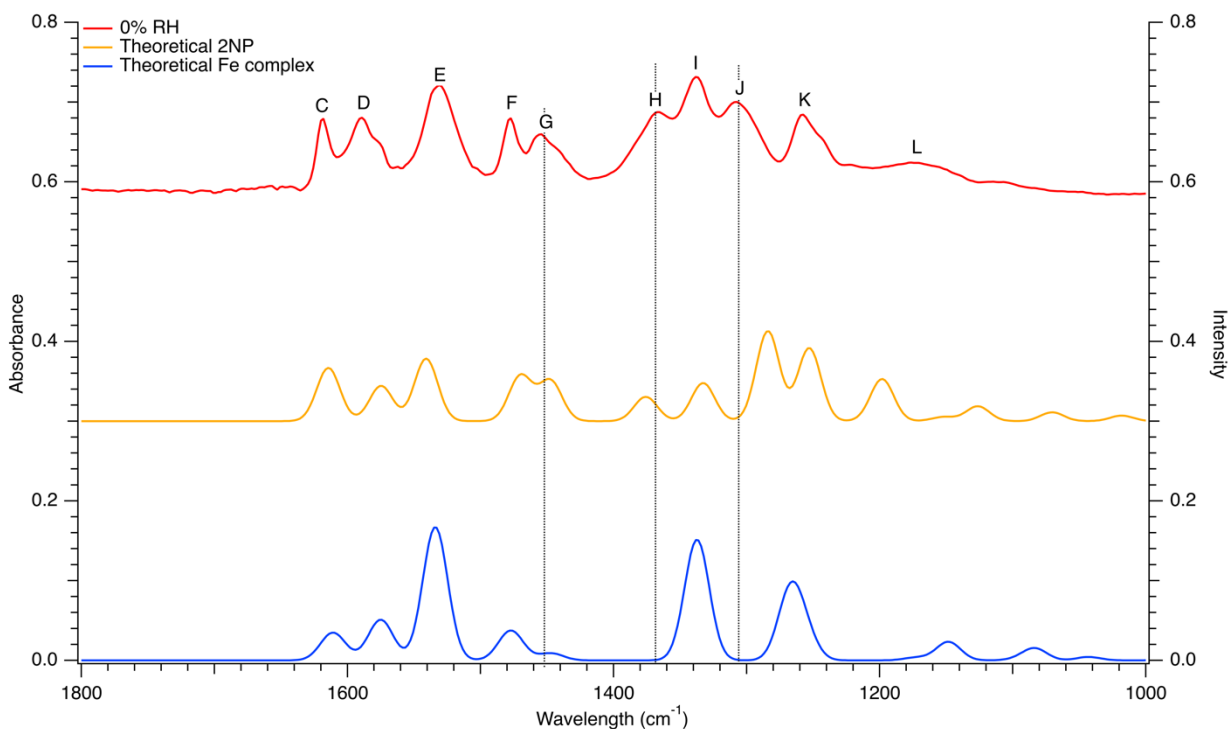


Figure 2.8: Gaussian calculations were performed to determine the theoretical spectra for gaseous 2NP and 2NP bonded to an aluminum structure. The blue spectrum is indicative of peaks from the 2NP bonded to the aluminum structure. The yellow spectrum is from the gas phase calculations. The red spectrum is from the experimental 0% RH.

The peaks in Figure 2.8 correspond with the peaks in Table 2.1. Peaks C-F are very consistent across all spectra because they vibrational motion associated with each of them is related to the ring structure of 2NP. The same is true for the peaks from K to the right. Three interesting peaks to note are G, H and J. Peak G represents the asymmetrical stretch of the ring and the functional groups, specifically the O-H bending. This motion is shown by Figure 2.9. This peak is noticeably different when the 2NP is chemisorbed to the iron structure due to vibrational motion

limitations imposed by the iron structure on that O-H bending. Thus, our experimental data is noticeably more like the physisorption model.

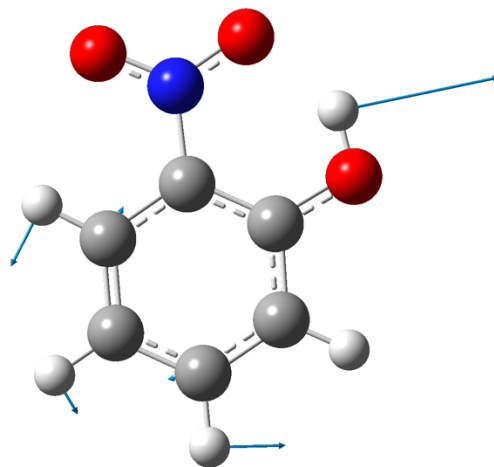


Figure 2.9: This figure shows the relative motion of the atoms on the 2NP molecule at the wavenumber  $1424\text{ cm}^{-1}$ , which is labeled peak G in Figure 2.8.

Another peak to look at is peak J. This peak again has to do with the stretching between the ring and functional groups. It is not present in the iron complex but appears to be present in the gas phase just at a lower wavenumber. This again leads us to believe that the likely method of interaction is physisorption. However, the best peak to confirm that physisorption is occurring is peak H. The complete lack of a peak here in the iron complex theoretical spectrum is a very good indication that our experimental data does not experience chemisorption. This peak is present in the gas so it's presence in our experimental data is very good confirmation that physisorption is the preferred interaction between 2NP and nontronite.

Something else to consider is the relative intensity of each peak. Overall, the intensities are more consistent with physisorption. However, there are some peaks within the chemisorption

spectrum that have a more relevant intensity. Peaks E and I have a more similar intensity to the chemisorption spectrum. This may indicate that there is some combination of physisorption and chemisorption occurring. We were not able to perform any combination calculations which might more accurately depict this, but that might be something worth exploring in the future.

While we have a strong indication of physisorption occurring, the similarities between the chemisorbed spectrum and the experimental spectrum should not be ignored. More data can be compared to further confirm the absence of chemisorption. For now, we can assume that physisorption is the primary method of adsorption, but some chemisorption may be occurring.

### *Relative Humidity*

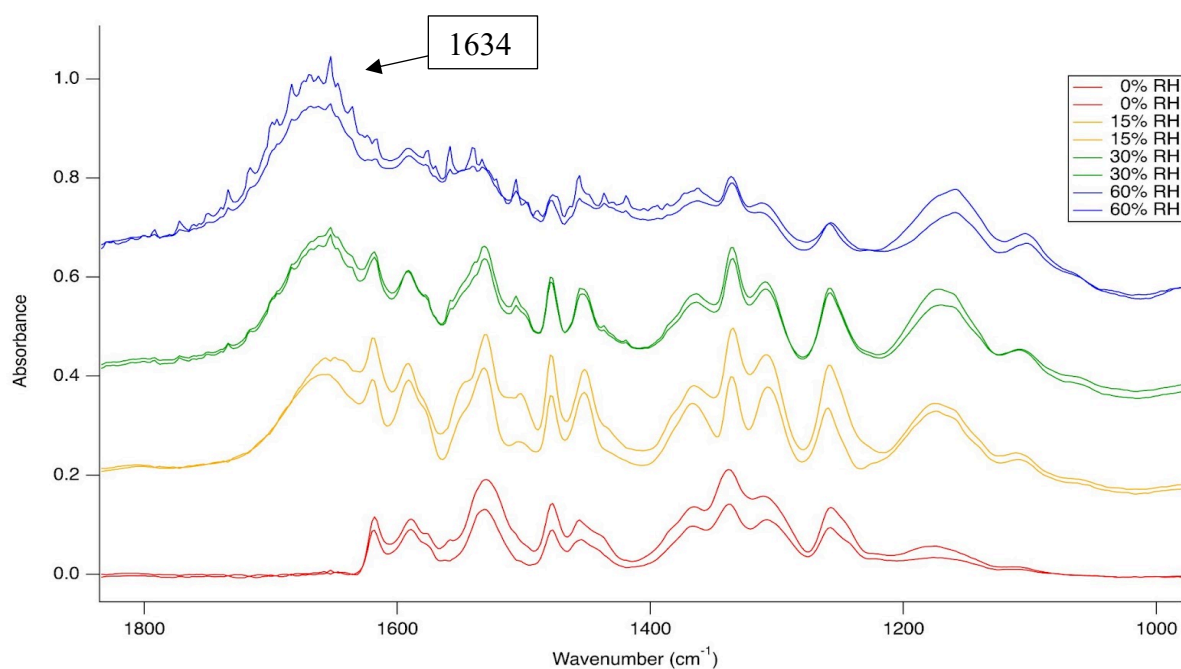


Figure 2.10: The graph shows the final spectrum for four different RHs, 60%, 30%, 15%, and 0% from top to bottom. It is zoomed into the fingerprint region to highlight the 2NP peaks. The

different RHs were shifted so that they weren't overlapping. The 60% was moved up to 0.65, 30% was shifted up to 0.4, 15% was shifted to 0.2, and the 0% was left at 0 absorbance.

With the assumption that physisorption is the primary method of adsorption, the next step was to examine how relative humidity affected adsorption. Water may also affect the O-H vibrations on nontronite, and relevant conditions in the atmosphere do not occur at 0% RH. Generally, there is a trend that as water adsorption increases, organic adsorption decreases. There is only a certain amount of area for adsorption to occur on the nontronite, meaning that if we add more water, there will be less room for the 2NP assuming only a monolayer is possible. Figure 2.10 shows the spectra for 4 different RHs. Each RH experiment was performed twice to corroborate the data. A peak at 1634 shows the water bending frequency. At higher humidities, this peak has a larger absorbance indicating that the relative humidity is increasing as we expect it to.

When comparing the different relative humidities with each other, we can see that 15% RH has a greater concentration of 2NP adsorbed to the surface. This is expressly noticeable around the 1300s  $\text{cm}^{-1}$ . In the past, we and other researchers have seen a consistent trend that as water adsorbs onto dust, adsorption of other molecules decreases dramatically. Nontronite is a swelling clay, meaning that as more water is exposed to the clay, water seeps in between the layers. Deng et al. describes how porosity of clays can impact VOC adsorption. While they did not test differing RH, they were able to see that montmorillonite, a clay very similar to nontronite, having greater porosity increased the adsorption of benzene onto it.<sup>26</sup> This swelling from the addition of water may increase porosity in nontronite and could account for the lack of decrease in 2NP. However,

it looks like 60% RH has less 2NP than 15% RH. There is variation between the relative humidities, but the 2NP does not fully disappear. This may mean that the porosity of the swelling clay is allowing for more 2NP adsorption than the water can displace. However, more research can be done to fully understand the trend that RH is having on the organic adsorption.

### *Photochemistry*

2NP is a photoreactive molecule, and we expected to see photochemistry occurring when the 2NP and nontronite were exposed to the solar simulator. Figure 2.11 shows the difference spectrum after the light was turned on. There was a clear loss of water seen in the OH bending region, around  $3400\text{ cm}^{-1}$  and at the water bending frequency,  $1634\text{ cm}^{-1}$ . Careful analysis shows that changes in the fingerprint region have the same kinetic profile to water loss. We believe the changes to be a result of shifted frequencies associated with drying and not chemistry. Integrating the 2NP peaks over time and comparing it to the water shows a similar trend. This graph shows that almost no interesting photochemistry is happening, but there is some correlation between the water and the 2NP.

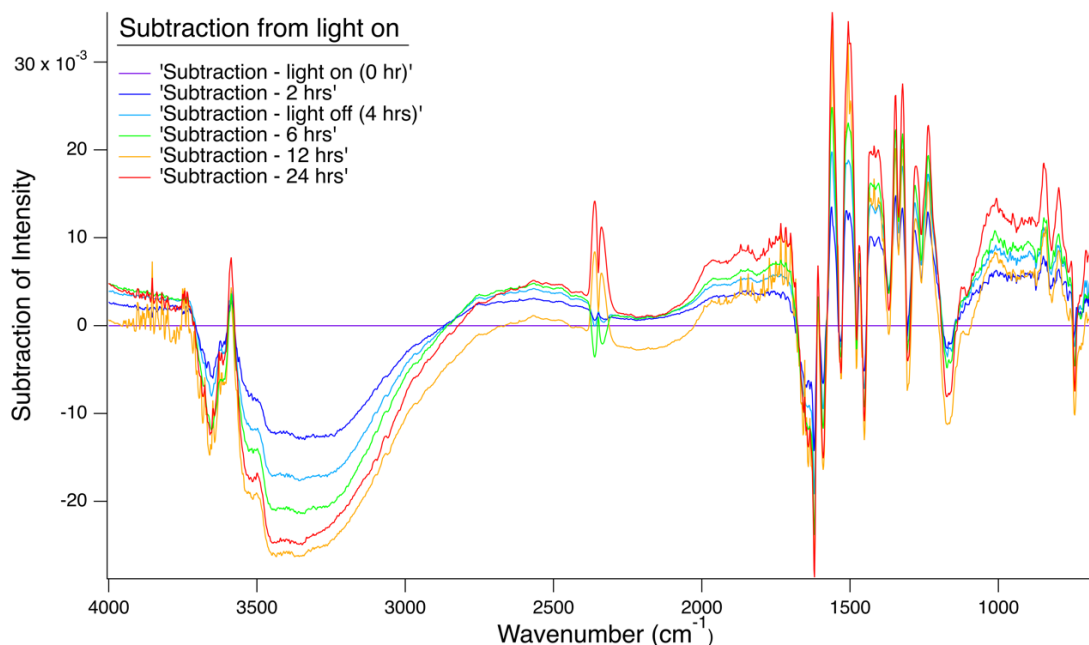


Figure 2.11: This graph shows the difference spectra of the light experiments. Each spectrum after the light was turned on was subtracted from the spectrum when the light was turned on (purple line). CO<sub>2</sub> was identified around 2330 cm<sup>-1</sup>. All other peaks are consistent with the previous spectra, where above 3000 cm<sup>-1</sup> is O-H stretching and below 1634 cm<sup>-1</sup> is the fingerprint region.

This result is similar to the results described in a paper by Tofan-Lazar and Al-Abadleh.<sup>11</sup> While working with the adsorption of catechol, a similarly relevant atmospheric compound, onto FeCl<sub>3</sub>, they found that RH had a greater effect on the photodecay of their compound than light and dark conditions did. Similarly, we are seeing a greater effect of RH on our compounds instead of light. However, this research saw a monodentate complex form between the catechol and onto FeCl<sub>3</sub>, which we are not seeing. They also saw photodecay, which we have not been able to see in our molecule. However, performing this photochemistry experiment at differing RH to see if we find similar results to this paper may be interesting for future research.

## **Chapter 3: Oceanographic distribution of phytoplankton and their nutrients**

### ***3.1: Introduction***

One of the most iron limited regions of the ocean is the Southern Ocean (SO). The SO likely gets nutrients from hydrothermal vents or upwelling.<sup>27</sup> There is some evidence of mineral dusts from Patagonia affecting the Atlantic sector of the SO.<sup>28</sup> Availability of nutrients is integral for phytoplankton. As the primary drivers of productivity in this region, phytoplankton distribution is critical to determining the overall productivity of the SO. The productivity in the SO is of extreme importance to oceanographers due to its ability to act as a CO<sub>2</sub> sink. This region process relies on the upwelling of bottom water and the subduction of surface water to sequester CO<sub>2</sub> in deep water. Phytoplankton known as coccolithophores are an important algal group for the sequestering of carbon in the SO.

### *Properties of the Southern Ocean*

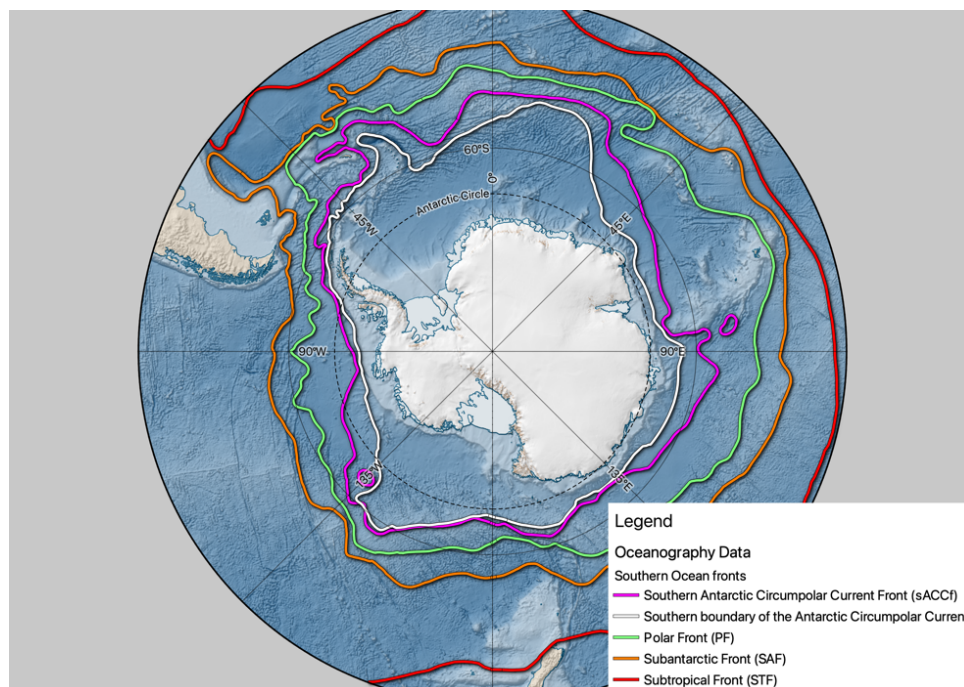


Figure 3.1: This figure shows the fronts and boundaries of major currents around Antarctica.<sup>29</sup>

The CO<sub>2</sub> uptake of the SO is affected by biota, which in turn is influenced by the physical properties of the area including currents and water mass properties. At places like fronts, which are areas where two distinct water masses meet, there are distinct changes in the nutrient availability and corresponding biota. The main current in the SO is the Antarctic Circumpolar Current (ACC), a strong eastward current. Several fronts surround Antarctica in concentric rings. In order from closest to farthest from Antarctica, they are the Southern ACC Front (SACCF), the Polar Front (PF), the Subantarctic Font (SAF), and the Subtropical Front (STF). The SAF is the northern-most boundary of the ACC, but the northern-most boundary of the SO is the STF, found around 40° S. The SAF is characterized by Subantarctic Mode Water (SAMW), which is estimated

to control around 75% of all biological productivity in regions north of 30° S. This water mass emerges in the SO but continues equatorward until it is subducted again at the equator. This water mass also contains the three types of phytoplankton that are of interest to us: coccolithophores, diatoms, and dinoflagellates.

Coccolithophores, diatoms, and certain dinoflagellates (Thoracosphaerids) are biomineralizing phytoplankton, meaning the phytoplankton can take certain nutrients and use them to precipitate mineralogenic shells. These shells can be helpful to the plankton in terms of ballasting or possibly protection against grazing.<sup>30</sup> Diatoms have long been categorized in the SO, specifically around the PF. Coccolithophores, however, have been categorized more recently from satellite data. Satellite imagery of the SO and light scattering calculations, show that there is a large swath of particulate inorganic carbon (PIC) in the SO around the Subantarctic front.<sup>31</sup> This PIC is mostly in the form of biomineralized shells of coccolithophores. Thus, this region has been termed the great calcite belt or GCB. Each of these phytoplankton, interacts differently in the SO.

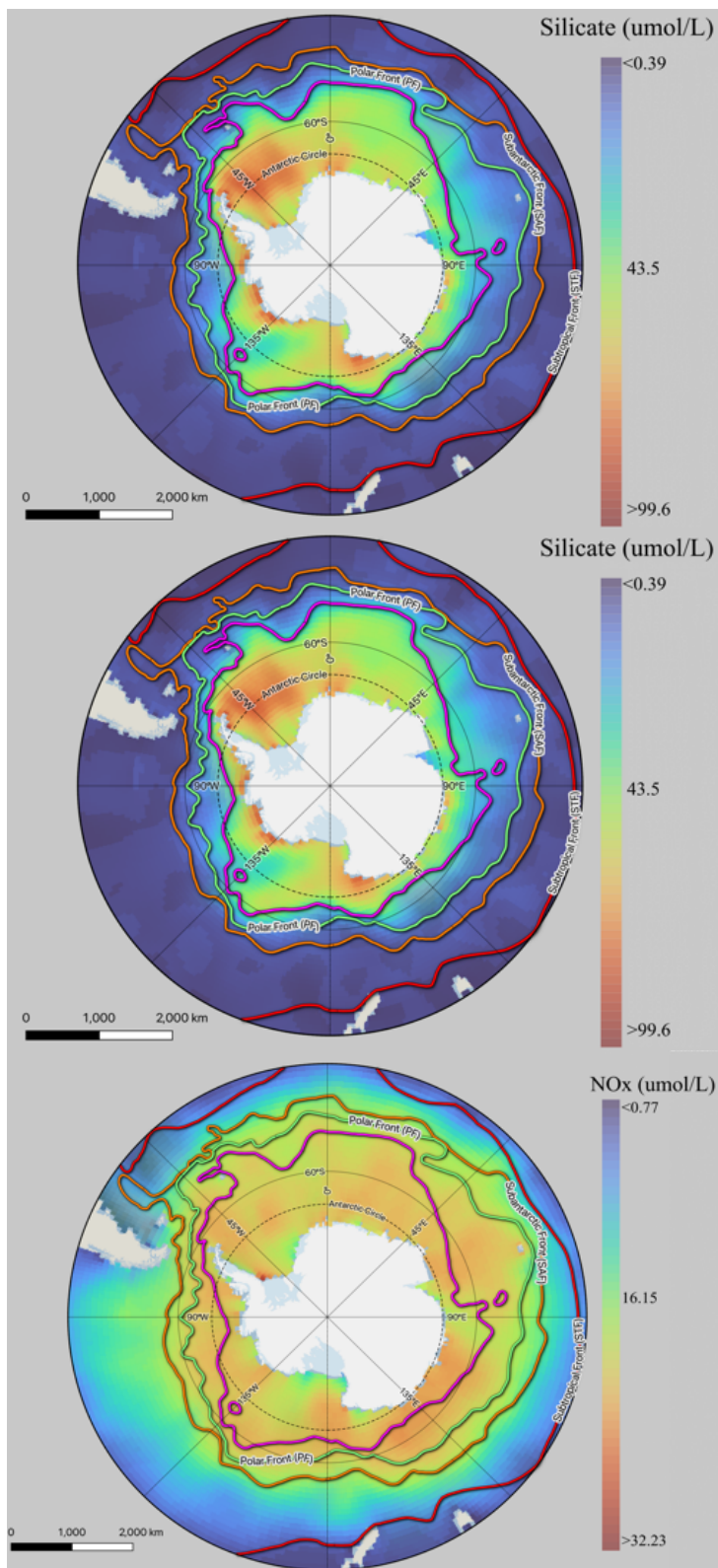


Figure 3.2: The figure shows the average modeled silicate (a), phosphate (b), and NOx (c) levels in  $\mu\text{mol/L}$  at the surface (25km) depth across the Southern Ocean.<sup>29,32</sup>

## *Diatoms*

Diatoms are a complex genus of phytoplankton with varying external silica-based shells or frustules. There is no exact number of species, and multiple groups have come up with different estimates. The most widely used estimate is approximately 200,000 different types of diatoms with approximately only 10,000 known species.<sup>33</sup> Conservative estimates place diatom species around 20,000. An updated number from the original group however, using new methods of extrapolation places the number of diatom species anywhere from 30,000 to 100,000.<sup>34</sup> Regardless of the exact number of possible diatoms, there are already around 12,000 known species. With the possibility of tens of thousands more species, it is safe to say that this group of phytoplankton is pretty variable. Each of these species has its own characteristics, and most of these revolve around the silica frustule shapes and structures.

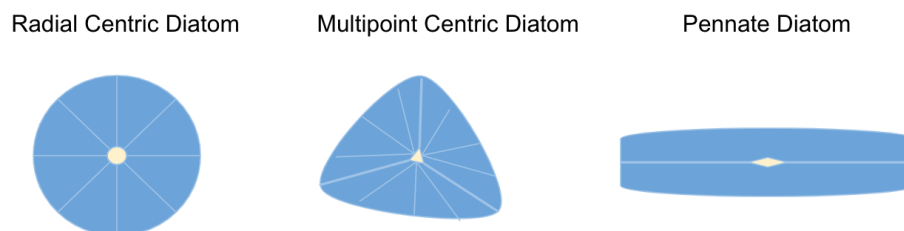


Figure 3.3: Examples of possible diatom shapes for radial centric, multipoint centric and pennate diatoms are provided above. These are general examples and do not describe all diatom shapes that fit into these categories.

Diatoms can be divided into groups based on structure for simplicity shown in Figure 3.3. Radial centric diatoms have circular frustules with a radial center and ribs extending from the

center. Multipolar centric diatoms have a similar radial center, but can have elongated, star-like, or multipoint structure. There are also pennate diatoms, which are elongated with an elongated center that the ribs extend from.<sup>30</sup> These can be simplified further based on symmetry into circular and pennate groups. Circular diatoms are radially symmetrical and pennate diatoms are bilaterally symmetrical. This paper concerns itself with radial centric and pennate diatoms as they were the most common observed in our SO work.

To produce these frustules, diatoms need silicic acid ( $\text{Si}(\text{OH})_4$ ) or “dissolved” silica. Silica transporters within the diatom can transport the silicic acid into the cell. In the cell, proteins and other possible molecules help the condensation from silicic acid to silica, which is used to build the frustules.<sup>35</sup> Silica present in the Southern Ocean comes from the sediment in the coast around Antarctica. This source of silica is why diatoms are so abundant in the SO. As shown in Figure 3.2, there is a drop-off of silica at the PF where diatoms are present. They condition the water to be much lower in silicate north of the PF, due to their necessity of taking up silicate in order to form their biogenic silica frustules and ultimately grow.

### ***Coccolithophores***

Coccolithophores are a calcifying phytoplankton group that make their structures out of calcium carbonate instead of silicate. These phytoplankton participate in calcium sequestration through the formation of calcite or calcium carbonate. Bicarbonate is taken up from the seawater and converted into calcium carbonate. This process takes place in a vesicle called the Golgi apparatus within the cell and is known as intracellular coccolithogenesis.<sup>30</sup> These plates are excreted to the outside of the cell where they build up and cover the entire organism to form a

matrix of calcium carbonate plates. This process of converting inorganic carbon to calcium carbonate is extremely important to the biogeochemistry of the SO, primarily performed by coccolithophores.

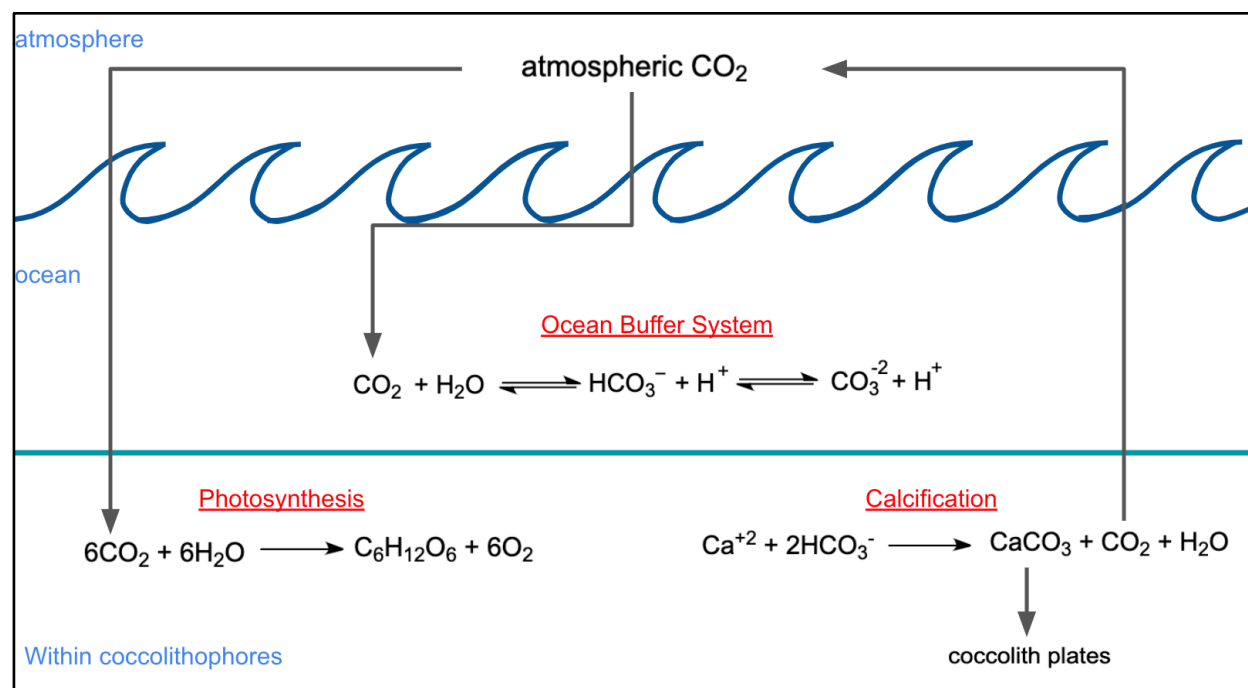


Figure 3.4: Diagram of carbon fluxes in relation to atmospheric and oceanic systems. Both photosynthesis and calcification for coccolithophores is depicted intracellularly.

Further, these coccoliths are eventually lost during processes such as reproduction and death. Many of the plates can sink out of the water column and eventually create layers in the sediment, leading to carbon sequestration. These layers of coccoliths in the sediments are important for geological studies. This process is important in terms of atmospheric levels CO<sub>2</sub> and

climate change because it is one of the few methods of sequestering inorganic carbon into the sediments.

Unlike diatoms, coccolithophores are more complicated regarding their morphological differences. Coccolithophores can be divided into two groups, heterococcoliths and holococcoliths.<sup>30</sup> The differences here are based in their crystal structure, and they do not come from different species but instead are thought to be different parts of the coccolithophore lifecycle. For the purposes of this work, we quantified coccolithophore abundance under the microscope based on their light scattering properties under polarized light.

### ***Dinoflagellates***

Thecae are an armor generally made of cellulose that most dinoflagellates have. There are some types that can be calciferous, however, but they are relatively rare. While the general formation of these shells does not rely on nutrient availability of waters, dinoflagellates are well known for their effects on water masses. Dinoflagellates are the main algae that participate in red tides and many species can produce toxins. Nutrient uptake by dinoflagellates in the SO can still impact the SAMW, regardless of whether the dinoflagellates are armored or not.

Dinoflagellates are divided into two groups for the purpose of identification in general and in terms of this work: armored and naked or unarmored. As one might expect, armored dinoflagellates have thecae and unarmored do not. Due to the extremely diverse nature of dinoflagellates, they were not identified from each other, but other plankton by their flagella and morphology. Two flagella are present in dinoflagellates. One of which forms a groove along the

equator of the plankton. This groove is the cingulum also referred to as a girdle. This groove is more evident in armored dinoflagellates but can also be seen in naked dinoflagellates.

### ***Plankton Importance and Experiments***

Biom mineralizing plankton change the nutrient availability in the water and essentially condition the SAMW before it moves equatorward. Understanding the relationships between nutrients and these phytoplankton groups is integral for understanding global nutrient availability, and the importance of SAMW on major ocean systems. Most coccolithophore data from the SO is satellite based. The research described here involved field measurements of the Indian Ocean sector of the SO, in an attempt to fill in some of the gaps of data on phytoplankton distribution. The remaining chapter focuses on phytoplankton count, distribution, and nutrient comparison data from the Southern Indian Ocean.

### ***3.2: Methods***

#### ***Location***

Data was collected by the crew and scientific party of the RV Thomas Thompson from the Southern Indian Ocean in December 2018 and January of 2019. Figure 3.3, provided in the Preliminary Cruise Report of the TN376 Thomas Thompson, shows the cruise track that was followed in this portion of the Great Calcite Belt. While data was collected along all these legs, the most notable sites for data collection came from leg 2, 4, and 5. Leg 2 and 5 both sampled a cyclonic eddy that had spun off of the Agulhas current. Leg 4 sampled a large swath of the great calcite belt that we could see in satellite data at different latitudes.

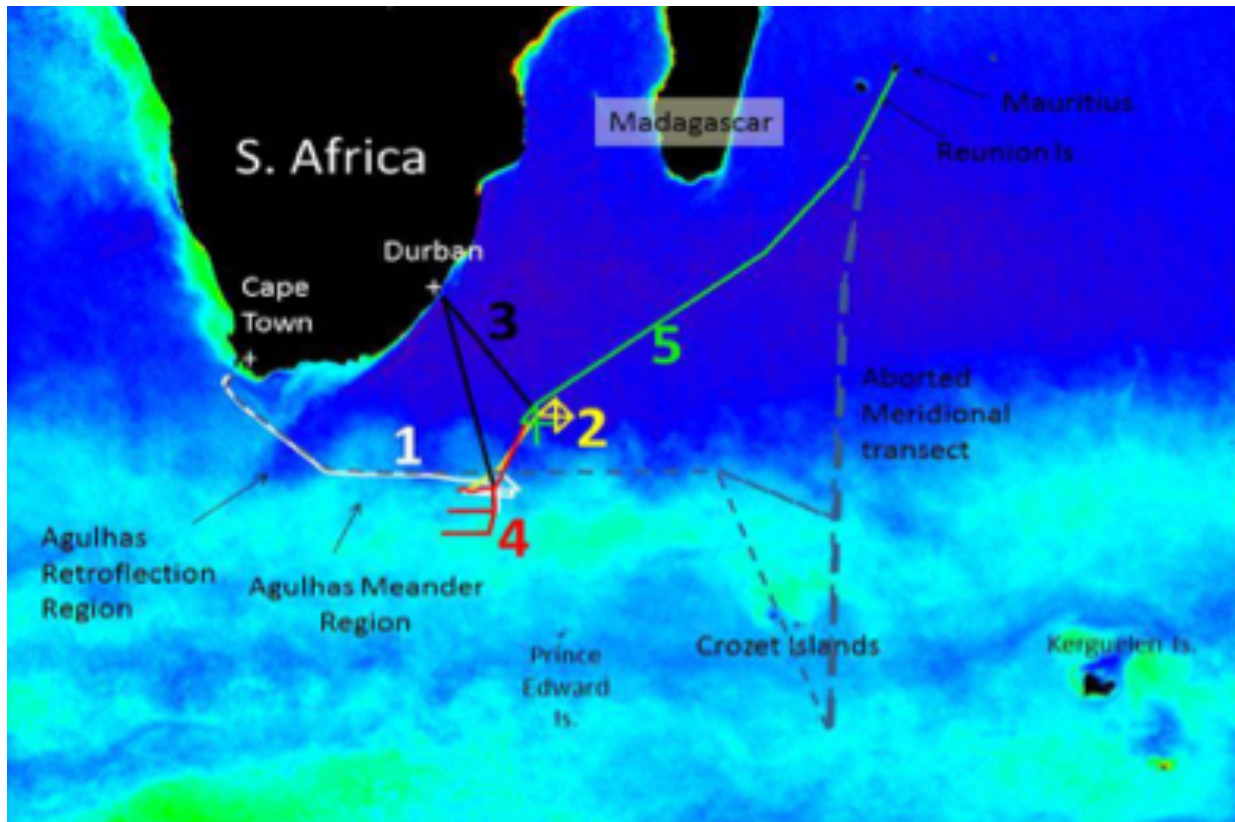


Figure 3.3: The cruise track denoted by the multicolored lines was broken down into five legs. Samples were taken from all legs of the cruise, but this essay focuses specifically on Leg 2 and 5. A cyclonic eddy had spun off from the Agulhas current and was sampled in a cross pattern twice shown in legs 2 and 5. This image comes from the preliminary cruise report.<sup>36</sup>

### *Water samples*

Water samples were collected using two methods; the primary method of water collection came from a CTD rosette. CTD stands for conductivity, temperature, and depth which are measured by the instrument in addition to collecting water. This rosette had 24 10L Niskin bottles. Each Niskin bottle was prepped, the ship was stopped, and then the CTD was deployed to the

desired depth. The final depth depended on the ocean floor depth. The second method was a method of underway sampling. Pipes carried water from the bow to the sink in the main lab. Phytoplankton analysis was done with two depths, the chlorophyll maximum and surface. All underway samples from the bow were counted as surface samples. The chlorophyll maximum is the depth where phytoplankton are abundant due to sunlight, nutrients, and other conditions. The chlorophyll max depth varied by region, but the surface samples were always ~5 meters.

Water was filtered in bulk using the setup shown in Figure 3.4. This setup was used to collect filters for biogenic silica (BSi), particulate inorganic carbon (PIC), particulate organic carbon (POC), cell counts, chlorophyll, and microscope slides. While all of these samples were collected in the same set-up, only microscope filter data will be considered in this work. Water was loaded into a 2-liter carboy, which was then set upside-down into a funnel over a filter. The samples were filtered under 5mm Hg vacuum to ensure the samples would finish filtering by the time when the next samples were ready. Filtrate was collected and discarded.

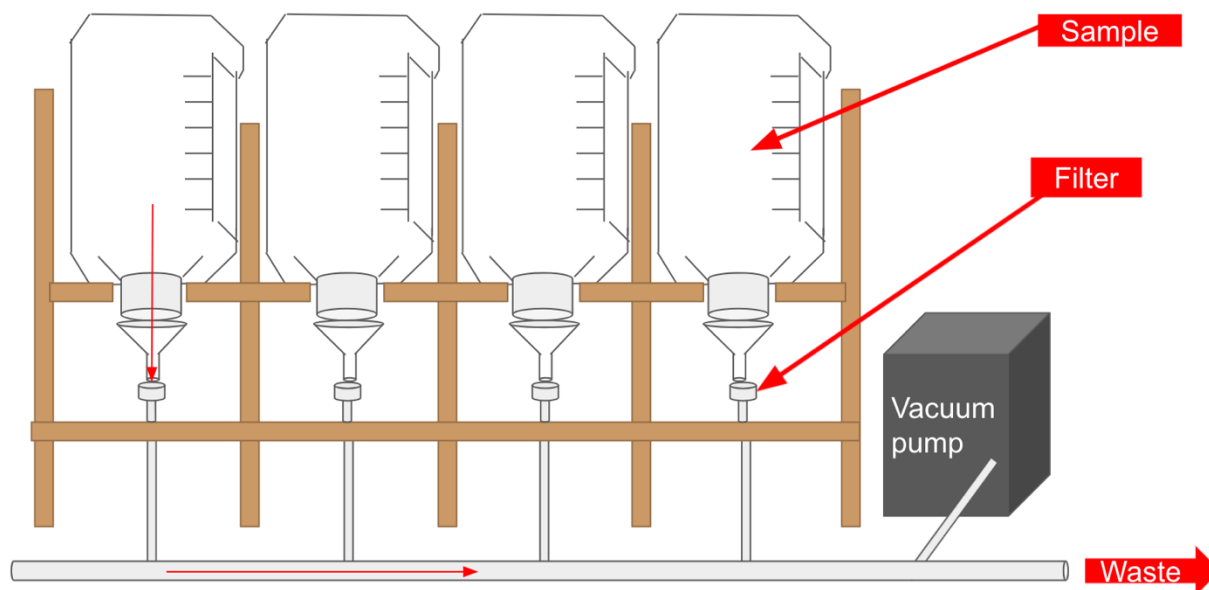


Figure 3.4: The filtration setup used consisted of 12 total bottles separated into 3 apparatuses, such as the one shown above. The bottles were placed upside-down on a specially made wooden holder, so that water was allowed to flow into a funnel, over a filter on a frit, and into waste tubing. The tubing was all connected to a vacuum pump to decrease filtration time.

### ***Microscope Imagery***

Microscope slides were prepared from this water using the filter-transfer-freeze (FTF) method.<sup>37</sup> Depending on the region and amount of phytoplankton within the area, either 100mL or 250 mL of water were used to prepare these samples. Water was filtered through a 25mm Nucleopore filters and was transferred to a microscope slide on a frozen block of metal kept at -80°C. Microscope slides were put under four different types of light: bright field, polarized, blue epifluorescence, and green epifluorescence. The different types of light allowed us to view different aspects of phytoplankton. Under polarized light, coccolithophores fluoresce. Under blue

epifluorescence, red fluorescence indicates chlorophyll, and lastly, under green epifluorescence, cyanobacteria fluoresce red. Pictures were taken of notable areas in the field to be studied later.

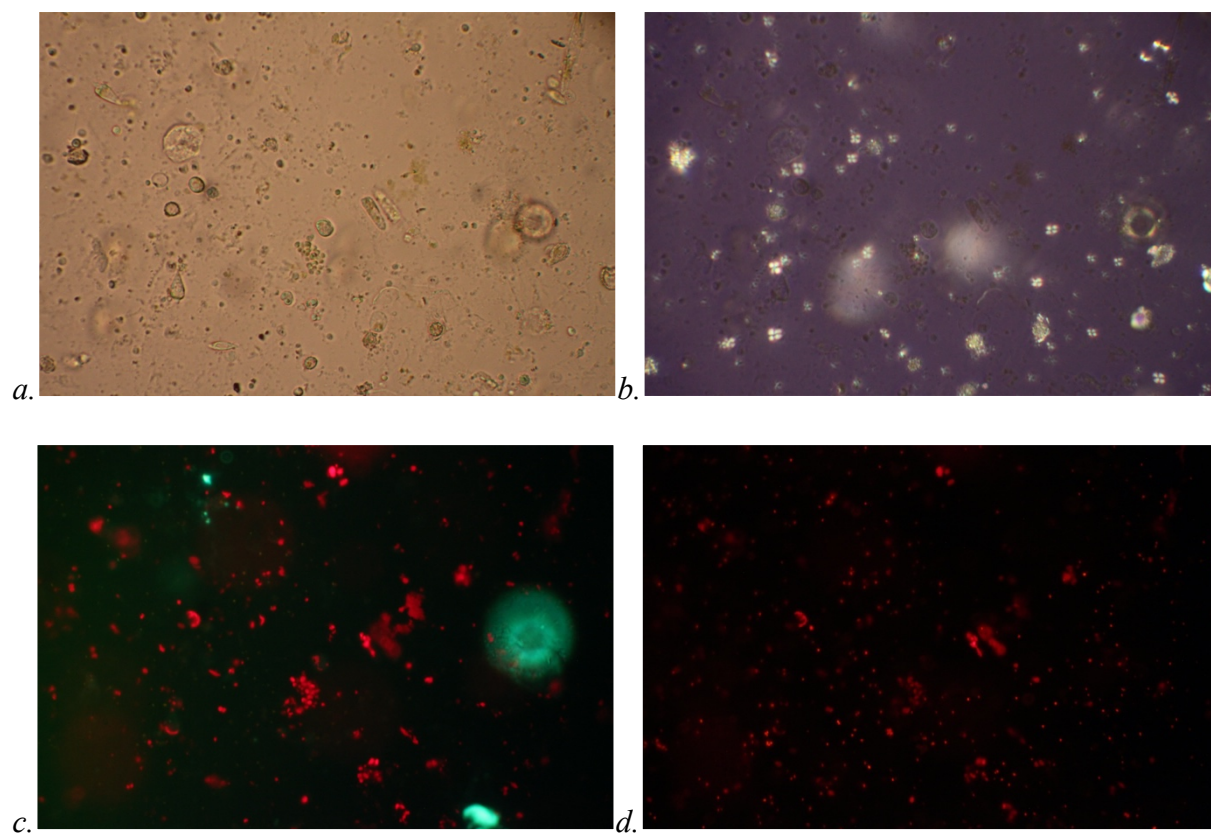


Figure 3.5: This figure shows microscope slides that were taken from station number 30 which was in a section from Leg 1 of the cruise. The bright field image (panel a) shows several phytoplankton including coccolithophores. The polarized light image (panel b) was used to identify coccolithophores and coccoliths. Panel c was used to identify chlorophyll-containing cells, denoted by the red fluorescence. These photographs were taken with blue epifluorescence with excitation at around 490nm. Image d was a photograph taken with green excitation at 530 nm to identify phycoerythrin-containing cyanobacteria.

The images taken of phytoplankton were calibrated for size. Generally, the images were taken at 400x magnification, which corresponded with images 187.5  $\mu\text{m}$  by 281  $\mu\text{m}$ . If a large enough phytoplankton warranted it, 200x magnification would be used, which corresponded with 375  $\mu\text{m}$  by 565  $\mu\text{m}$ . The filter itself had an area of 8.31  $\text{cm}^2$ . Using the image area, filter area, and total volume of sea water filtered, the concentration of phytoplankton in the total sample was extrapolated. The fractional area of field per total effective filtered area for 400x and 200x magnification was  $6.34 \times 10^{-5}$  and  $2.55 \times 10^{-4}$  respectively.

Phytoplankton were identified based on major characteristics specific to each type. Diatoms were classified based on their structure in bright field images. Chains of diatoms were not counted together, and the diatoms were counted into the subcategories: pennate or centric. When data was analyzed, all subcategories of diatoms were included into one diatom category. Dinoflagellates were also identified in the bright field image based on morphology. Generally, dinoflagellates were identified by a girdle. They were divided into armored or naked categories but combined into one dinoflagellate category for analysis. Coccolithophores were identified in the bright field and the polarized light images. Coccolithophores were also identified by plates in the bright field and a white fluorescence in the polarized light images. No phytoplankton were identified to a species level.

Each station had two to three depths that were analyzed under the microscope. On average, 42 images were analyzed per depth, but each depth had a different number of images. Twelve depths were analyzed all from the cyclonic eddy. The images were loaded into ImageJ and FIJI.<sup>38</sup> FIJI specifically was used to tag cells by hand with the multipoint tool.

### *Nutrient Analysis*

Water for nutrient samples was collected the same as the water for the microscope slides. Samples from the same bottles and depths were run through a Seal Analytical continuous-flow AutoAnalyzer 3 (AA3) provided and operated by Scripps Institute of Oceanography.<sup>39</sup> Nutrient data was corroborated by other measurements taken by the CTD and provided to the entire science party. Nutrients analyzed in this manner were nitrates ( $\text{NO}_3^-$ ), nitrites ( $\text{NO}_2^-$ ), phosphates ( $\text{PO}_4^{3-}$ ), silica ( $\text{Si}(\text{OH})_4$ ), and ammonium ( $\text{NH}_4^+$ ). For the purposes of this essay,  $\text{Si}(\text{OH})_4$  will be referred to as silicate for short.

### 3.3: Results

#### *Phytoplankton Types*

	Diatoms	Coccolithophores	Dinoflagellates	Cells
1 <sup>st</sup> sampling	3	167	158	8916
2 <sup>nd</sup> sampling	5	106	83	2121
Total cells	8	273	241	11037

Table 3.1: The table above shows the total cells found in all slides at all depths at all stations. It includes the cell counts from the first sampling of the eddy and the second sampling as well as the total

The second sampling only included two sampling sites whereas the first sampling included three sampling sites, which meant that there was more data for the first sampling. While we cannot compare numbers of cells between samplings, we can compare the different ratios of phytoplankton groups to each other. Diatoms were extremely low, totaling 8 out of 11037 cells. Due to the lack of diatoms, analysis was not conducted between this group and others. Because the eddy was located further north than the SAF, it makes sense that we would not see many diatoms in this low silica area far from the PF. Further comparisons of phytoplankton groups were conducted by determining the log of cells/mL of each type and comparing them, as shown in Figure 3.6. The logarithmic transformation was used because phytoplankton are typically log-normally distributed.

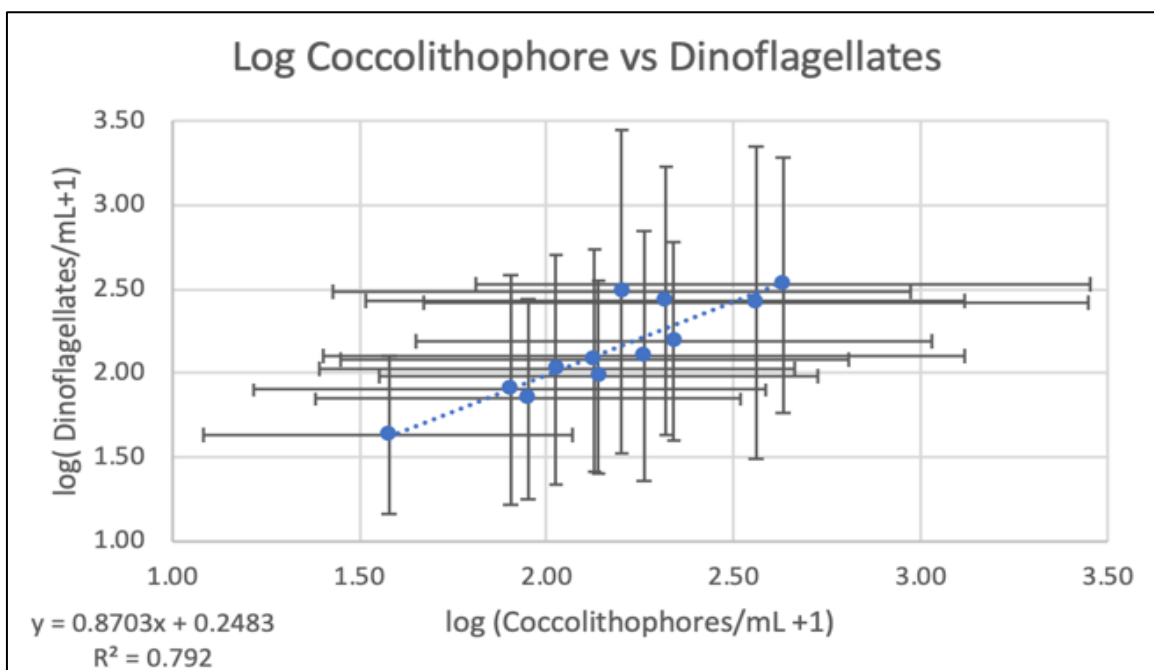


Figure 3.6: Cell comparisons were made by determining the log of each cell count per station and graphing the different phytoplankton types against each other. This graph shows the comparison of coccolithophores and dinoflagellates in the areas sampled.

Phytoplankton follow a log scale distribution, so for the purpose of our research, the log was taken of the cell/mL data, and one was added to all the data to account for any images that had no phytoplankton present. The linear graphs shown in Figure 3.6 was generated from such log-transformed data. The figure shows the relation of coccolithophores and dinoflagellates. There was an observed almost 1:1 ratio between the coccolithophores and phytoplankton. These results are significant and encouraging. Most of our observations while collecting this data indicated that this was likely, and it proved to be the case. This ratio was consistent across multiple sampling sites across the SO.

### *Phytoplankton Depth Distribution*

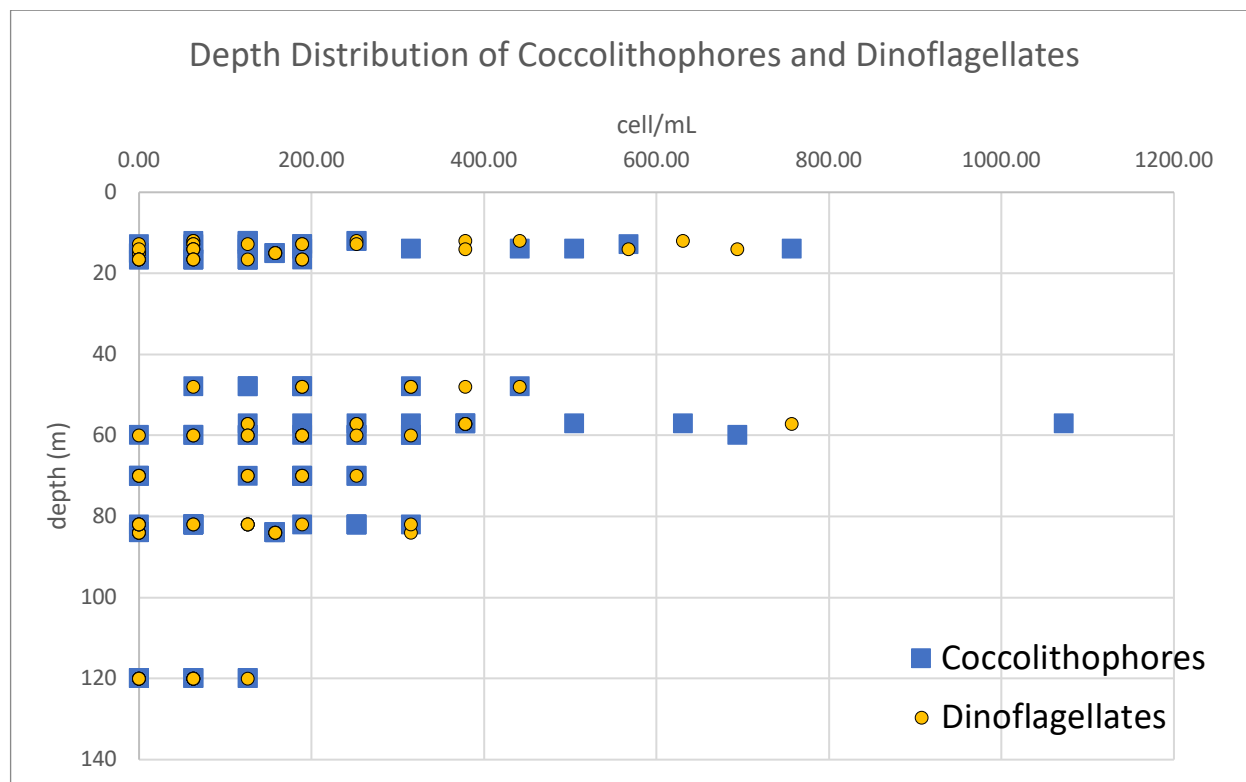


Figure 3.7: Phytoplankton concentrations in cells per milliliter were plotted against depth. Again, diatoms were excluded due to their extremely low numbers.

Dinoflagellates and coccolithophores were in almost equal amounts present at surface and chlorophyll maximum depths. Additionally, coccolithophores and dinoflagellates were present in almost the same amounts at the same depths, which was also seen in Figure 3.7. This trend between coccolithophores and dinoflagellates was expected based on the data from Figure 3.6. This data allows us to see that the 1:1 ratio of coccolithophores and dinoflagellates was consistent at differing depths.

### Nutrient Analysis

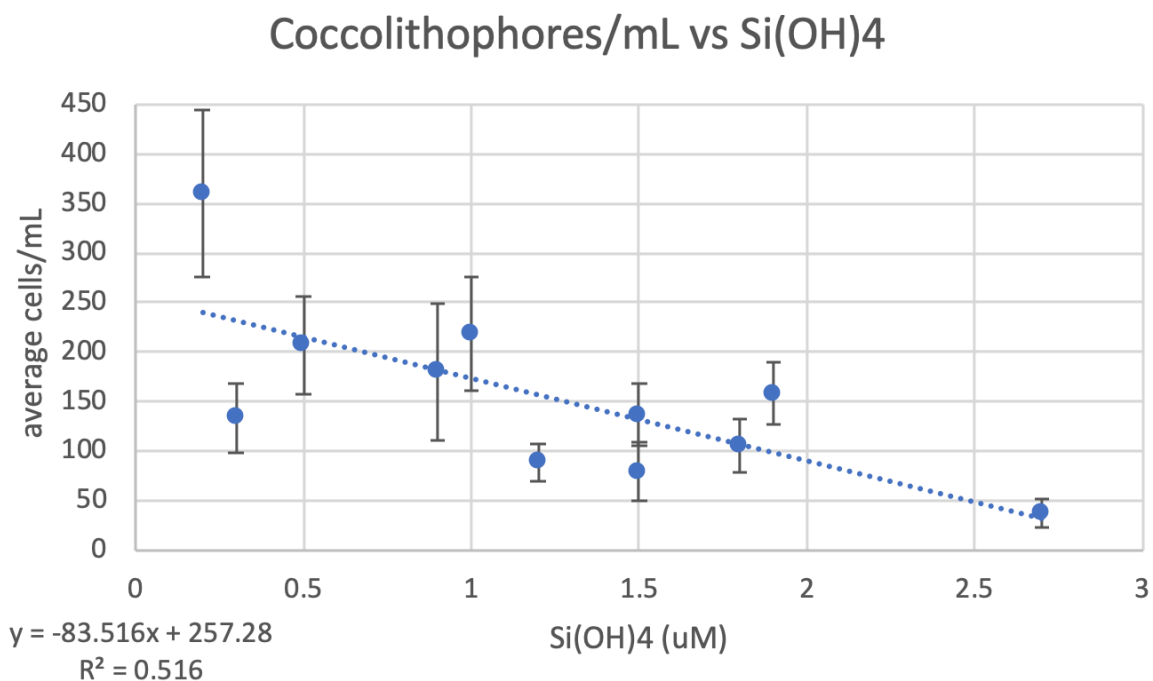


Figure 3.8: This graph shows the average cells per milliliter of coccolithophores plotted against the concentration in millimolar of silica. The line of best fit was generated, and the equation of the line can be found in the bottom left of the graph.

Each of the phytoplankton were compared directly to each nutrient that we analyzed, including nitrates, nitrites, phosphates, silica, and ammonia. However, the only statistically significant data was between the coccolithophores and the silica nutrients. This data was unexpected. In terms of silica distribution, waters closer to Antarctica have higher concentrations, because the deep ocean in this area is a source of silica as shown in Figure 3.2.<sup>32</sup> This silica distribution is correlated with the phytoplankton distribution. Diatoms, being heavily dependent on silicate, are closer to Antarctica and pull most of the silica out of the water column before it can

reach more northern latitudes in the SO. We did not see enough diatoms in our samples to expect any statistically significant data between the diatoms and silica nutrients. However, it is unexpected that we would see coccolithophores being statistically negatively related to silicate, given that they are not thought to require silica for growth, but they do need calcite for their coccolith formation. Indeed, coccolithophores appear to need a minimum amount of silica for growth, but the picture may be more complicated.

A paper by Durak et al. saw that there was a possible pathway that coccolithophores have for the silica transport within the cell.<sup>40</sup> Silica transporters allow for the uptake of silica to places where silica may condense in diatoms to be made into frustules. Silica transporters have been shown to be present in several species of coccolithophore, but the absolute role still appears to be enigmatic.

It is also interesting that we do not see a statistically significant trend with dinoflagellates and silica, especially because their distribution appears to be closely related to coccolithophores. This may imply that there is something specifically with the coccolithophores that is influencing the trend in Fig. 3.8. One possibility is that the negative slope in Fig. 3.8 represents some degree of competition between coccolithophores and diatoms (where diatoms would be more abundant at higher silicate levels). However, more work is necessary to make any significant conclusions.

## Chapter 4: Discussion

### *4.1: A review*

The interactions between the ocean and atmosphere have vast reaching implications for our world. Atmospheric reactions between organic molecules, like 2NP, and mineral dusts, like nontronite, can impact the properties of mineral dusts or the organic molecule. The mineral dust then settles out in the ocean and can leech important limiting nutrients, such as iron, into the ocean. Iron and other limiting nutrients control the population growth and distribution of phytoplankton. Phytoplankton are the primary producers of the ocean, the base of the marine food chain, and they can have impacts on alkalinity and O<sub>2</sub>/CO<sub>2</sub> levels in the ocean. Phytoplankton in the SO are likely impacted by nutrient availability in the SAMW around the SAF.

Our research looking at the interactions between 2NP and nontronite found that physisorption was the primary method of adsorption. We also found relative humidity to play an almost insignificant role in the adsorption of 2NP onto nontronite. In addition, we saw no significant photochemistry. The research about the phytoplankton distribution in the SO concluded that the relationship between dinoflagellates and coccolithophores was approximately a 1:1 ratio. From this we can conclude that these two groups may require the same nutrient availability to coexist. Additionally, the only significant data that we found was between silica and coccolithophores. There may be several explanations for this. One explanation could be a need for silica uptake by coccolithophores.

## ***4.2: Relationship between the two projects***

### ***Location***

The Sahara is the largest source of dust-based bioavailable iron in the Atlantic Ocean. However, it does not extend to all the world's oceans. Of the total global number of mineral dust aerosols, the southern hemisphere only makes about 10%. Of this 10%, the two largest sources of mineral dust in the southern hemisphere are from Australia (approx. 120 Tg/yr) and South America (approx. 50 Tg/yr).<sup>41</sup> Because of the strong winds of this region, dust is blown eastward from each continent, effectively giving South American mineral dust control of the Atlantic sector of the SO and the Australian mineral dust control over the Pacific sector of the SO. Desert soils are generally classified as Aridisols or Entisols, which can put the smectite composition anywhere from 5-20% in the topsoil.<sup>42</sup> Smectites are present in abundance in the topsoil of Eastern Australia. In South America, smectites are more abundant in the subsoil, but they still appear in the topsoil. Mineral dust may be sparse in the SO and its effect may be small, but there is a noticeable probability of smectites like nontronite being swept out over the SO. Despite the vast differences between these two projects, there is still some overlap regarding geographic location. While iron was not a nutrient that we measured in the phytoplankton project, it would be interesting to relate iron levels to phytoplankton distribution in the SO along with likely sources of mineral dust in the SO.

### ***Relative Humidity***

We found that nontronite has a variable amount of adsorbance by 2NP depending on RH. The most interesting aspect of this is that there is not a linear relationship between RH and adsorbance. We expected to see adsorbance decrease as RH increases, because water molecules

may adsorb to the surface first and allow for the solvation of 2NP. While we see 60% RH has the lowest adsorbance, 15% and 30% RH do not follow the trend. 15% has the highest adsorbance. This trend should be investigated further, due to the relevance of changing humidity in this area. With aerosol dust starting in very low humidity regions (deserts) and moving to high humidity regions (oceans), this data shows that the adsorption of VOCs could vary greatly.

As discussed in chapter 2, nontronite is a swelling clay, likely the cause of the trend in our data. As water and 2NP seep in between the layers, there is more surface area for the 2NP to adsorb to and interact with. All smectites are swelling clays, which indicates that they should follow this same trend. A study using smectites, specifically montmorillonite and beidellite, as a possible surface for styrene removal found something similar. While the study added certain organic groups to help aid the adsorbance of styrene, the best adsorbance was found at 40-50% RH, and there was a notable decrease in adsorbance at 80% RH.<sup>43</sup> They attribute this trend to the swelling nature of the clays, which corroborates our own data. Interestingly, the average RH in most deserts is 40% or less and the RH over the ocean can be around 80%. This may indicate that more meaningful interactions are happening over land in terms of VOC adsorption to swelling clays than over the ocean.

### ***Oxidation State***

One of the classic questions of iron availability from mineral dust deals with oxidation state. Smectites can have either a +3 or +2 charge on the iron. In soils, microbes can change the oxidation state, but other compounds like sulphates have the ability to reduce a ferric nontronite.

<sup>44</sup> Studies have been done on the reduction of ferric iron in nontronite by many compounds, including nitroaromatic compounds.<sup>45</sup> In our case, when looking at the photoreactivity and spectra

of 2NP, we did not observe any oxidation. While there may be some other factors that we do not see happening, we can say that our data did not suggest a reduction of nontronite. We entered these experiments thinking that 2NP and nontronite could be a good proxy but based on our observations, there is likely a better model that can be used. While further research could be done to observe the oxidation state, it may be better to look at different dust and organic interactions.

Another interesting aspect of oxidation state is that a change in oxidation state of iron can change surface area and swelling properties of smectites. Ferrous nontronite swells less than ferric nontronite.<sup>46</sup> Extrapolating from our data, we may infer that swelling would still have an effect of the ferrous nontronite, but not to the same extent that we see here. If swelling is lessened in the ferrous state, that may show a significant decrease in 2NP peaks in the presence of higher RH, which we expected to see but did not see. With a decrease swelling, this may decrease total adsorption.

### ***Nutrients***

These mineral dusts also contain silica, which we were able to see a good correlation within the plankton data. The SO is not limited by dissolved silica. The main sources of silica in this area are from the meltwaters of Antarctica.<sup>47</sup> However, mineral dust is a very small source of silica in the SO (<0.005 Tmol/yr).<sup>47</sup> The rest of the global oceans however receive about 0.5 Tmol/yr of silica from mineral dust.<sup>47</sup> Despite the availability of silica in the SO, a large portion is used up by the Polar front where diatoms congregate. North of the polar front, silica levels decrease, but mineral dust sources become closer. To my knowledge, there is no silica concentration data at

different areas in the SO. Perhaps mineral dust becomes a greater source of silica north of the PF in the SO. More work should be done to investigate this.

Understanding the biogeochemical cycling of nutrients is a greatly important undertaking. By studying the aeolian sources of iron and silica, we can relate it to nutrients and nutrient availability's importance in the SO. We focused on swelling clays, specifically nontronite, due to its availability and iron concentration. Our data highlights the variability of 2NP adsorption onto smectites in the presence of differing relative humidities. After 30% RH, we saw a decrease in adsorption, due to the swelling characteristics of the clay. However, there is data to suggest that a more reactive form a nontronite that has ferrous iron, would have different swelling properties, and change implications for iron dissolution and 2NP adsorption. While iron is known to be a limiting nutrient across the globe, we also found a clear important trend between coccolithophores and dissolved silica. Mineral dust is a minor source of dissolved silica in the global ocean and an even smaller source in the SO. However, north of the PF, silica levels drop again, and mineral dust may be able to fill in the gaps of this area. Of course, this data can be improved upon, through the collection of more data in the SO for iron and silica levels based on frontal boundaries. This could help distinguish where silica and iron are most limiting in the SO.

### ***4.3: Future Research***

There are many aspects of ocean and atmospheric interaction that can be studied more. From this work alone, we identified adsorption mechanisms and relative humidity trends that can be researched more when looking at the interactions of 2NP and nontronite. Additionally, the relationship between coccolithophores and silica was identified to be a significant trend, but the reasoning for this should be investigated further. The overlap between these two projects can also be expanded upon. Additional research on swelling clays as an important source of iron and silica should be conducted while taking iron charge and swelling into account. Other types of nontronite should be explored to see if the possible tetrahedral coordinated irons impact the chemistry. The geographic location of available iron mineral dust can be studied to compare with the geographic location of phytoplankton and their overall distribution. Given this information, we could draw further conclusions about nutrients, iron, and phytoplankton in the SO and improve our understanding of atmospheric and oceanic interdependence.

## Bibliography

- (1) Martin, J. H.; Fitzwater, S. E. Iron Deficiency Limits Phytoplankton Growth in the North-East Pacific Subarctic. *Nature* **1988**, *331* (6154), 341–343.  
<https://doi.org/10.1038/331341a0>.
- (2) Jickells, T. D.; An, Z. S.; Andersen, K. K.; Baker, A. R.; Bergametti, G.; Brooks, N.; Cao, J. J.; Boyd, P. W.; Duce, R. A.; Hunter, K. A.; Kawahata, H.; Kubilay, N.; laRoche, J.; Liss, P. S.; Mahowald, N.; Prospero, J. M.; Ridgwell, A. J.; Tegen, I.; Torres, R. Global Iron Connections Between Desert Dust, Ocean Biogeochemistry, and Climate. *Science* **2005**, *308* (5718), 67–71. <https://doi.org/10.1126/science.1105959>.
- (3) Tegen, I.; Fung, I. Modeling of Mineral Dust in the Atmosphere: Sources, Transport, and Optical Thickness. *Journal of Geophysical Research Atmospheres* **1994**, *99*.  
<https://doi.org/10.1029/94JD01928>.
- (4) Modeling the Mineralogy of Atmospheric Dust Sources. *Journal of Geophysical Research: Atmospheres* **1999**, *104* (D18), 22243–22256.  
<https://doi.org/10.1029/1999JD900416>.
- (5) Perlwitz, J. P.; Pérez García-Pando, C.; Miller, R. L. Predicting the Mineral Composition of Dust Aerosols – Part 1: Representing Key Processes. *Atmospheric Chemistry and Physics* **2015**, *15* (20), 11593–11627. <https://doi.org/10.5194/acp-15-11593-2015>.
- (6) Kandler, K.; Schütz, L.; Deutscher, C.; Ebert, M.; Hofman, H.; Jäckel, S.; Jaenicke, R.; Knippertz, P.; Lieke, K.; Massling, A.; Petzold, A.; Schladitz, A.; Weinzierl, B.; Zorn, S.; Weinbruch, S. Size Distribution, Mass Concentration, Chemical and Mineralogical

- Composition and Derived Optical Parameters of the Boundary Layer Aerosol at Tinfou, Morocco, during SAMUM 2006. *Tellus* **2009**, *61*, 32–50.
- (7) Veghte, D. P.; Freedman, M. A. Facile Method for Determining the Aspect Ratios of Mineral Dust Aerosol by Electron Microscopy. *Aerosol Science and Technology* **2014**, *48* (7), 715–724. <https://doi.org/10.1080/02786826.2014.920484>.
- (8) Mahowald, N. M., A. R. Baker, G. Bergametti, N. Brooks, R. A. Duce, T. D. Jickells, N. Kubilay, J. M. Prospero, and I. Tegen (2005), Atmospheric Global Dust Cycle and Iron Inputs to the Ocean, *Global Biogeochem. Cycles*, *19*, GB4025, Doi:10.1029/2004GB002402.
- (9) *The Biological Productivity of the Ocean | Learn Science at Scitable.*  
<https://www.nature.com/scitable/knowledge/library/the-biological-productivity-of-the-ocean-70631104/> (accessed 2021-11-26).
- (10) Morsink, K. *With Every Breath You Take, Thank the Ocean | Smithsonian Ocean.*  
<http://ocean.si.edu/ocean-life/plankton/every-breath-you-take-thank-ocean> (accessed 2021-11-26).
- (11) Tofan-Lazar, J.; Al-Abadleh, H. A. Surface Water Enhances the Uptake and Photoreactivity of Gaseous Catechol on Solid Iron(III) Chloride. *Environmental Science & Technology* **2014**, *48* (1), 394–402. <https://doi.org/10.1021/es404321s>.
- (12) Tofan-Lazar, J.; Situm, A.; Al-Abadleh, H. A. DRIFTS Studies on the Role of Surface Water in Stabilizing Catechol–Iron(III) Complexes at the Gas/Solid Interface. *The Journal of Physical Chemistry A* **2013**, *117* (40), 10368–10380. <https://doi.org/10.1021/jp406113r>.

- (13) Chin, H.; Hopstock, K. S.; Fleming, L. T.; Nizkorodov, S. A.; Al-Abadleh, H. A. Effect of Aromatic Ring Substituents on the Ability of Catechol to Produce Brown Carbon in Iron(III)-Catalyzed Reactions. *Environ. Sci.: Atmos.* **2021**, *1* (2), 64–78. <https://doi.org/10.1039/D0EA00007H>.
- (14) Wang, L.; Wang, X.; Gu, R.; Wang, H.; Yao, L.; Wen, L.; Zhu, F.; Wang, W.; Xue, L.; Yang, L.; Lu, K.; Chen, J.; Wang, T.; Zhang, Y.; Wang, W. Observations of Fine Particulate Nitrated Phenols in Four Sites in Northern China: Concentrations, Source Apportionment, and Secondary Formation. *Atmospheric Chemistry and Physics* **2018**, *18* (6), 4349–4359. <https://doi.org/10.5194/acp-18-4349-2018>.
- (15) Hinrichs, R. Z.; Buczek, P.; Trivedi, J. J. Solar Absorption by Aerosol-Bound Nitrophenols Compared to Aqueous and Gaseous Nitrophenols. *Environmental Science & Technology* **2016**, *50* (11), 5661–5667. <https://doi.org/10.1021/acs.est.6b00302>.
- (16) Hems, R. F.; Abbatt, J. P. D. Aqueous Phase Photo-Oxidation of Brown Carbon Nitrophenols: Reaction Kinetics, Mechanism, and Evolution of Light Absorption. *ACS Earth and Space Chemistry* **2018**, *2* (3), 225–234. <https://doi.org/10.1021/acsearthspacechem.7b00123>.
- (17) Paris, R.; Desboeufs, K. V.; Journet, E. Variability of Dust Iron Solubility in Atmospheric Waters: Investigation of the Role of Oxalate Organic Complexation. *Atmospheric Environment* **2011**, *45* (36), 6510–6517. <https://doi.org/10.1016/j.atmosenv.2011.08.068>.
- (18) Chen, H.; Grassian, V. H. Iron Dissolution of Dust Source Materials during Simulated Acidic Processing: The Effect of Sulfuric, Acetic, and Oxalic Acids. *Environmental Science & Technology* **2013**, *47* (18), 10312–10321. <https://doi.org/10.1021/es401285s>.

- (19) Angelini, M. M.; Garrard, R. J.; Rosen, S. J.; Hinrichs, R. Z. Heterogeneous Reactions of Gaseous HNO<sub>3</sub> and NO<sub>2</sub> on the Clay Minerals Kaolinite and Pyrophyllite. *The Journal of Physical Chemistry A* **2007**, *111* (17), 3326–3335. <https://doi.org/10.1021/jp0672656>.
- (20) Nickovic, S.; Vukovic, A.; Vujadinovic, M.; Djurdjevic, V.; Pejanovic, G. Technical Note: High-Resolution Mineralogical Database of Dust-Productive Soils for Atmospheric Dust Modeling. *Atmospheric Chemistry and Physics* **2012**, *12* (2), 845–855. <https://doi.org/10.5194/acp-12-845-2012>.
- (21) Keeling, J.; Raven, M.; Gates, W. Geology and Characterization of Two Hydrothermal Nontronites from Weathered Metamorphic Rocks at the Uley Graphite Mine, South Australia. *Clays and Clay Minerals* **2000**, *48*, 537–548. <https://doi.org/10.1346/CCMN.2000.0480506>.
- (22) Bejan, I.; Abd-el-Aal, Y.; Barnes, I.; Benter, T.; Bohn, B.; Wiesen, P.; Kleffmann, J. The Photolysis of Ortho-Nitrophenols: A New Gas Phase Source of HONO. *Phys Chem Chem Phys* **2006**, *8* (17), 2028–2035. <https://doi.org/10.1039/b516590c>.
- (23) Barsotti, F.; Bartels-Rausch, T.; De Laurentiis, E.; Ammann, M.; Brigante, M.; Mailhot, G.; Maurino, V.; Minero, C.; Vione, D. Photochemical Formation of Nitrite and Nitrous Acid (HONO) upon Irradiation of Nitrophenols in Aqueous Solution and in Viscous Secondary Organic Aerosol Proxy. *Environ. Sci. Technol.* **2017**, *51* (13), 7486–7495. <https://doi.org/10.1021/acs.est.7b01397>.
- (24) *List and Availability of Special Clay Minerals*. <https://www.agry.purdue.edu/cjohnston/sourceclays/specialclays.htm> (accessed 2022-02-21).

- (25) *Phenol, 2-nitro-*. <https://webbook.nist.gov/cgi/inchi?ID=C88755&Mask=80> (accessed 2021-12-02).
- (26) Deng, L.; Yuan, P.; Liu, D.; Annabi-Bergaya, F.; Zhou, J.; Chen, F.; Liu, Z. Effects of Microstructure of Clay Minerals, Montmorillonite, Kaolinite and Halloysite, on Their Benzene Adsorption Behaviors. *Applied Clay Science* **2017**, *143*, 184–191. <https://doi.org/10.1016/j.clay.2017.03.035>.
- (27) Schine, C. M. S.; Alderkamp, A.-C.; van Dijken, G.; Gerringa, L. J. A.; Sergi, S.; Laan, P.; van Haren, H.; van de Poll, W. H.; Arrigo, K. R. Massive Southern Ocean Phytoplankton Bloom Fed by Iron of Possible Hydrothermal Origin. *Nat Commun* **2021**, *12* (1), 1211. <https://doi.org/10.1038/s41467-021-21339-5>.
- (28) Anderson, R. F.; Barker, S.; Fleisher, M.; Gersonde, R.; Goldstein, S. L.; Kuhn, G.; Mortyn, P. G.; Pahnke, K.; Sachs, J. P. Biological Response to Millennial Variability of Dust and Nutrient Supply in the Subantarctic South Atlantic Ocean. *Philosophical Transactions of the Royal Society A: Mathematical, Physical and Engineering Sciences* **2014**, *372* (2019), 20130054. <https://doi.org/10.1098/rsta.2013.0054>.
- (29) Matsuoka, K.; Skoglund, A.; Roth, G. *Quantarctica*, 2018. <https://doi.org/10.21334/NPOLAR.2018.8516E961>.
- (30) Knoll, A. H.; Falkowski, P. G. *Evolution of Primary Producers in the Sea*; Academic Press: Amsterdam, 2007.
- (31) Balch, W. M.; Bates, N. R.; Lam, P. J.; Twining, B. S.; Rosengard, S. Z.; Bowler, B. C.; Drapeau, D. T.; Garley, R.; Lubelczyk, L. C.; Mitchell, C.; Rauschenberg, S. Factors Regulating the Great Calcite Belt in the Southern Ocean and Its Biogeochemical

- Significance. *Global Biogeochemical Cycles* **2016**, *30* (8), 1124–1144.  
<https://doi.org/10.1002/2016GB005414>.
- (32) Garcia, H. E., R. A. Locarnini, T. P. Boyer, J. I. Antonov, O. K. Baranova, M. M. Zweng, J.R. Reagan, D. R. Johnson, 2013. World Ocean Atlas 2013. Vol. 4: Dissolved Inorganic Nutrients (Phosphate, Nitrate, Silicate). S. Levitus, Ed.; A. Mishonov, Technical Ed. NOAA Atlas NESDIS 76, 25 Pp.
- (33) Mann, D. G.; Droop, S. J. M. 3. Biodiversity, Biogeography and Conservation of Diatoms. *Hydrobiologia: The International Journal of Aquatic Sciences* **1996**, *336* (1–3), 19.  
<https://doi.org/10.1007/bf00010816>.
- (34) Mann, D. G.; Vanormelingen, P. An Inordinate Fondness? The Number, Distributions, and Origins of Diatom Species. *J. Eukaryot. Microbiol.* **2013**, *60* (4), 414–420.  
<https://doi.org/10.1111/jeu.12047>.
- (35) Yang, W.; Lopez, P.; Rosengarten, G. Diatoms: Self Assembled Silica Nanostructures, and Templates for Bio/Chemical Sensors and Biomimetic Membranes. *The Analyst* **2010**, *136*, 42–53. <https://doi.org/10.1039/c0an00602e>.
- (36) Balch, W. Cruise Science Report: TN376 R/V Thomas G. Thompson : Preliminary Cruise Summary of R/V THomas G THompson TN#376 Presentint Cruise Narratice and Reports of Each Group within the Science Party. **2020**, 130.
- (37) Hewes, C.; Holm-Hansen, O. A Method for Recovering Nanoplankton from Filters for Identification with the Microscope: The Filter-Transfer-Freeze (FTF) Technique. *Limnol. Oceanogr.* **1983**, *28* (2), 389–394.

- (38) Schindelin, J.; Arganda-Carreras, I.; Frise, E.; Kaynig, V.; Longair, M.; Pietzsch, T.; Preibisch, S.; Rueden, C.; Saalfeld, S.; Schmid, B.; Tinevez, J.-Y.; White, D. J.; Hartenstein, V.; Eliceiri, K.; Tomancak, P.; Cardona, A. Fiji: An Open-Source Platform for Biological-Image Analysis. *Nature Methods* **2012**, *9* (7), 676–682.  
<https://doi.org/10.1038/nmeth.2019>.
- (39) *Dissolved Inorganic Nutrient Analysis Procedure*. Scripps Institution of Oceanography.  
<https://scripps.ucsd.edu/ships/shipboard-technical-support/odf/documentation/nutrient-analysis> (accessed 2021-11-15).
- (40) Durak, G. M.; Taylor, A. R.; Walker, C. E.; Probert, I.; de Vargas, C.; Audic, S.; Schroeder, D.; Brownlee, C.; Wheeler, G. L. A Role for Diatom-like Silicon Transporters in Calcifying Coccolithophores. *Nature Communications* **2016**, *7* (1), 10543.  
<https://doi.org/10.1038/ncomms10543>.
- (41) Li, F.; Ginoux, P.; Ramaswamy, V. Distribution, Transport, and Deposition of Mineral Dust in the Southern Ocean and Antarctica: Contribution of Major Sources. *Journal of Geophysical Research: Atmospheres* **2008**, *113* (D10).  
<https://doi.org/10.1029/2007JD009190>.
- (42) Ito, A.; Wagai, R. Global Distribution of Clay-Size Minerals on Land Surface for Biogeochemical and Climatological Studies. *Sci Data* **2017**, *4* (1), 170103.  
<https://doi.org/10.1038/sdata.2017.103>.
- (43) Matusik, J.; Koteja-Kunecka, A.; Maziarz, P.; Kunecka, A. Styrene Removal by Surfactant-Modified Smectite Group Minerals: Efficiency and Factors Affecting

- Adsorption/Desorption. *Chemical Engineering Journal* **2022**, 428, 130848.  
<https://doi.org/10.1016/j.cej.2021.130848>.
- (44) Neumann, A.; Sander, M.; Hofstetter, T. B. Redox Properties of Structural Fe in Smectite Clay Minerals. In *ACS Symposium Series*; Tratnyek, P. G., Grundl, T. J., Haderlein, S. B., Eds.; American Chemical Society: Washington, DC, 2011; Vol. 1071, pp 361–379.  
<https://doi.org/10.1021/bk-2011-1071.ch017>.
- (45) Hofstetter, T.; Schwarzenback, R.; Haderlein, S. Reactivity of Fe(II) Species Associated with Clay Minerals. *Environ. Sci. Technol.* **2003**, 37, 519–528.
- (46) Lear, P. R.; Joseph; Stucki, W. Effects of Iron Oxidation State on the Specific Surface Area of Nontronite. *Clays and Clay Minerals* **1989**, 37 (6), 547–552.
- (47) Tréguer, P. J. The Southern Ocean Silica Cycle. *Comptes Rendus Geoscience* **2014**, 346 (11), 279–286. <https://doi.org/10.1016/j.crte.2014.07.003>.